RGNZ/MGPB

Integrated Geophysical Constraints on Crustal Structure and Along-Strike Heterogeneity beneath Java Island, Southern Sunda Arc

Rudarsko-geološko-naftni zbornik
(The Mining-Geology-Petroleum Engineering Bulletin)
DOI: 10.17794/rgn.2026.5.1

Original scientific paper

Rian Amukti[1,2]*, Rashad A Bantan[1], Hamdy Aboulela[1,3], Lina Handayani[2], Sonny Aribowo[2]

[1] *Faculty of Marine Geology, King Abdulaziz University, Jeddah, Saudi Arabia, 21589.*
[2] *National Research and Innovation Agency (BRIN), Bandung, Indonesia, 10340.*
[3] *Faculty of Science, Suez Canal University, Ismalilia, Egypt, 8366004.*

Abstract

Southern and central Java are situated along the Sunda–Java subduction system, where interactions among slab geometry, crustal structure, and upper-plate deformation govern regional tectonics and seismicity. Our study presents an integrated geophysical pattern, stress orientations, gravity anomalies, Moho depth variations, and subsurface structures beneath Java. The area spans approximately 106° E-114 °E and 7°S-10°S. We combine earthquake catalog data from 2000-2023 (48,825 events, magnitude range 2.7-7.8 mb, depth range 10-600 km) obtained from USGS data, focal mechanism solutions, event-based stress orientations, satellite-derived gravity data, Radially Averaged Power Spectrum (RAPS) analysis for Moho depth estimation, and two-dimensional seismic reflection profiles. The seismicity distribution depicts a northward-dipping Wadati-Benioff zone and reveals a relative reduction in earthquake occurrence at intermediate depths beneath Central Java. Gravity analysis reveals systematic lateral variations in crustal density and thickness, with high anomalies along the southern margin, low anomalies beneath sedimentary basins, and local high anomalies associated with volcanic regions. RAPS analysis indicates that the Moho depth ranges from approximately 11 to 40 km, consistent with previous regional studies. Seismic reflection profiles document reflector discontinuities and fault-related deformation consistent with frontal, back-arc, and strike-slip fault systems within the Sunda-Java margin.

Keywords:
Sunda-Java subduction; Seismicity; Focal Mechanism; Gravity Anomaly; Moho Depth (RAPS)

1. Introduction

Java Island lies along the southern edge of the Sunda Plate within one of the world's most active subduction settings, where the Indo-Australian Plate moves northward beneath Southeast Asia. Key tectonic components of the Sunda-Java margin, namely the Sunda Trench, a mature Wadati-Benioff seismic zone, an active Quaternary volcanic arc, and a back-arc deformation province, have been well documented by decades of geological, seismological, and geodetic investigations (**Hutchings & Mooney, 2021; Schlüter et al., 2002; Simandjuntak, 1993; Simandjuntak & Barber, 2016**). Gravity, seismic reflection, and receiver-function studies further demonstrate systematic variations in crustal thickness and density from the trench to the back-arc region (**Green et al., 1981; Handayani et al., 2022; Hanif et al., 2024; Syuhada & Anggono, 2016**).

Even with this established understanding, important aspects of crustal and lithospheric geodynamics beneath southern Java remain unresolved. Recent tomography and catalog-based studies report reduced intermediate-depth seismicity south of central Java (a "seismic gap") and interpret it as evidence for slab segmentation or slab rearing in the subducting Indo-Australian Plate (**Widiyantoro et al., 2020, 2022, 2024**). Such interpretations raise key questions about slab continuity and stress transmission, and their implications for upper-plate deformation, particularly along the Java Back-Arch Thrust. However, most studies have addressed these processes chiefly from seismicity or tomographic perspectives, while the mechanical links among slab geometry, stress field, crustal thickness, and active faulting have not been assessed comprehensively in an integrated geophysical framework.

This knowledge gap is particularly critical in light of the rising seismic activity along southern Java and the large, densely distributed population exposed to earthquake and tsunami hazards. Focal mechanism analyses have revealed along-strike variations in faulting style across the Sunda Java margin (**Patria & Aulia Nur,**

* Corresponding author: Rian Amukti
e-mail address: rian.amukti87@gmail.com
Received: 14 October 2025. Accepted: 3 March 2026.
Available online: 26 October 2026

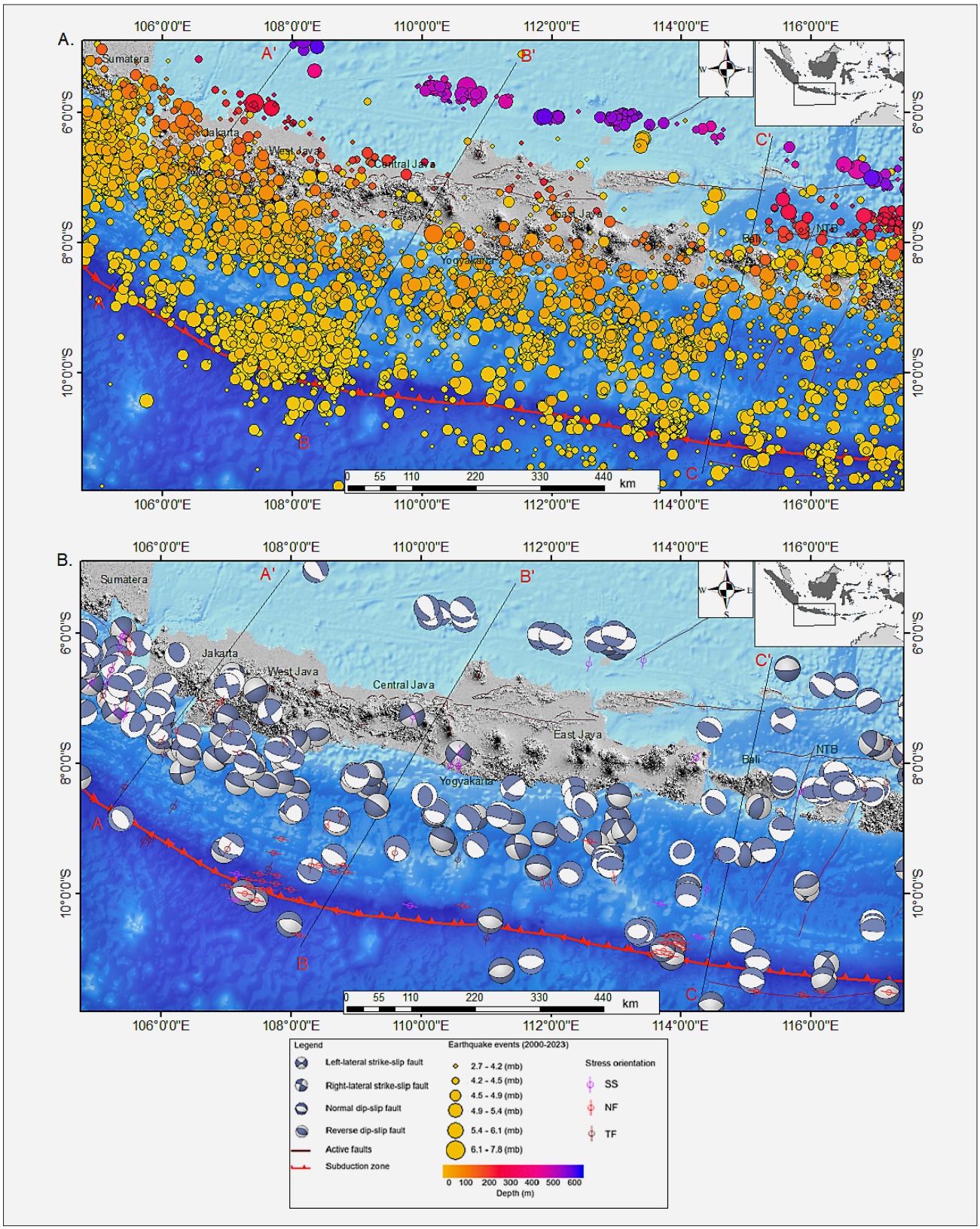


Figure 1: (a) Seismicity map of the study area across the Southern Sunda Arc, earthquake data from the USGS catalog (2000–2023). (b) Focal mechanisms and stress indicators for the same region. Beachball symbols represent focal mechanism solutions (Mb 4.0–7.0; 2011–2023). Colored symbols show event-based stress-regime indicators derived from focal mechanisms: strike-slip (SS) in purple, normal faulting (NF) in red, and thrust faulting (TF) in brown. The Sunda–Java subduction zone/trench axis is highlighted in bright red. Black lines A–A′, B–B′, and C–C′ mark the locations of trench-perpendicular cross-section profiles used to project earthquake hypocenters and analyze depth-dependent seismicity patterns in Figure 2, source: (**Heidbach et al., 2018; Helmholtz-Zentrum Potsdam, 2024; USGS, 2023**).

2020; Supendi et al., 2018), while gravity-based studies have mapped regional density contrasts and basin architecture (**Handayani et al., 2022**). However, the datasets are typically treated in isolation. In addition, post-2020 resources, including updated earthquake catalogs, revised stress-field compilations, and newly available seismic reflection data, have not yet been synthesized into a single, coherent tectonic interpretation for southern Java.

This study overcomes this limitation by examining southern and central Java within an area approximately bounded by 106 ° E-114 ° E and 7 ° S- 10 ° S. The study region spans the Sunda-Java Trench, the forearc and volcanic arc domains, and the northern back-arc zone where the Java Back-Arc Thrust is expressed (see **Figure 1**). This area coincides spatially with the seismic gap and slab segmentation zone proposed by **Widiyantoro et al.** (**2020, 2022, 2024**) and benefits from the availability of multiple complementary geophysical datasets.

The objective of the study is not to reiterate the presence of subduction, fault systems, and the Moho beneath Java, as these features are already well established. Rather, we seek to refine and consolidate existing understanding by investigating the mechanical links among slab segmentation, stress distribution, crustal thickness variations, and active faulting beneath southern Java. This is accomplished by integrating: (1) earthquake seismicity and focal-mechanism data (2000-2023); (2) stress-field constraints derived from focal mechanisms and the World Stress Map; (3) gravity-anomaly analyses, including spectral estimates of Moho depth; and (4) interpretation of two-dimensional seismic reflection data. The main contribution of this work is a unified synthesis of these datasets within a consistent spatial framework, enabling a more comprehensive evaluation of crustal architecture and tectonic segmentation along the southern Sunda Arc.

2. A seismic and Tectonic Sketch

The Southern Sunda Arc constitutes a mature convergent margin formed by the northward subduction of the Indo-Australian Plate beneath the Sunda Plate. From south to north, the principal tectonic elements include the Sunda–Java Trench, an accretionary prism and forearc basin, the Quaternary volcanic arc, and a back-arc domain affected by compressional and transpressional deformation. Regional seismicity outlines a continuous, northward-dipping Wadati–Benioff zone extending to depths exceeding 600 km, reflecting the geometry of the subducting slab beneath Java (**Hutchings & Mooney, 2021**).

Earthquake focal mechanism studies indicate systematic variations in faulting style across the margin (see **Figure 1**). Thrust-fault mechanisms dominate near the trench and shallow plate interface, reflecting interplate compression, whereas normal-fault and strike-slip mechanisms occur more frequently beneath the volcanic arc and within the subducting slab, associated with slab bending, internal deformation, and back-arc stress regimes (**Patria & Aulia Nur, 2020; Supendi et al., 2018**). These variations highlight along-strike and cross-arc heterogeneity in tectonic processes.

Seismic tomography indicates a complex slab geometry beneath southern Java, with low-velocity anomalies and locally disrupted slab continuity that have been interpreted as evidence of slab weakening, segmentation, or tearing (**Widiyantoro et al., 2020, 2022, 2024**). These anomalies coincide spatially with areas of reduced intermediate-depth seismicity, although the mechanical implication of this association remains under debate.

Gravity and receiver function results further suggest pronounced spatial variability in crustal thickness across Java, with thicker crust in central Java and progressive thinning toward the trench and the northern back arc (**Handayani et al., 2022; Syuhada & Anggono, 2016**). Within the upper plate, shortening is active along the Java Back-Arc Thrust (**Aribowo et al., 2022**), and focal mechanisms together with seismicity indicate continuing compression consistent with subduction-related stress transmission (**Supendi et al., 2018**).

In combination, these lines of evidence establish a coherent seismic and tectonic framework for the Southern Sunda Arc. We use this framework as the starting point for the present study, which integrates seismicity, stress information, gravity-derived constraints (including Moho depth), and seismic reflection interpretation to sharpen constraints on the spatial arrangement and mechanical connections among these tectonic elements beneath southern Java.

3. Methods

3.1. Study Area and Spatial Extent

We focus on southern and central Java, Indonesia, covering approximately 106 °E-114 °E and 7°S-10°S. This region includes the Sunda-Java Trench, the forearc basin, the Quaternary volcanic arc, and the northern back-arc zone where the Java Back-Arc Thrust (JBT) has developed. The chosen area aligns with zones of notable slab heterogeneity and seismic segmentation previously identified beneath Java (**Hutchings & Mooney, 2021; Widiyantoro et al., 2020, 2022, 2024**). It is further supported by the availability of the multiscale geophysical data required for integrated crustal-lithospheric analysis.

3.2. Seismicity and Focal Mechanism Data

Earthquake records were obtained from the United States Geological Survey (USGS) catalog for 2000-2023 (**USGS, 2023**). The dataset includes 48,825 events, spanning magnitudes of M 2.7-7.8 and focal depths of

10-600 km. While this interval does not capture a full megathrust seismic cycle, earlier work suggests that multi-decade catalogs are adequate for identifying first-order seismicity patterns, depth-dependent distributions, and relative seismic gaps in subduction zones (**Hayes et al., 2018; Hutchings & Mooney, 2021**).

We used focal mechanism solutions from the GEOFON Program (Helmholtz-Zentrum Potsdam), which reports centroid moment tensor (CMT) solutions for moderate-to-large earthquakes (**Dziewonski et al., 1981; Ekström et al., 2012**). Faulting style was then assigned as reverse, normal, or strike-slip by considering the nodal-plane orientation and the geometry of the P and T axes, in line with standard seismotectonic approaches (**Heidbach et al., 2018; Zoback, 2010**).

Global catalogs were preferred over local networks due to their consistent magnitude scaling, uniform quality control, and regional completeness, which allow straightforward comparisons along the Sunda-Java margin (**Hayes et al., 2018**). We analyzed epicentral distribution, depth structure, and clustering to define the Wadati-Benioff zone, assess upper-plate deformation, and map relative reductions in seismicity density. Here, such reductions are presented strictly as observations and are not used as direct proxies for seismic hazard or slab tearing.

3.3. Stress Field Analysis

Stress orientation and relative magnitude were estimated using focal-mechanism data together with the World Stress Map compilation (**Heidbach et al., 2010, 2018**). Focal mechanism inversion, supported by numerical modelling, was used to determine the prevailing SHmax orientation across Java.

Recent studies indicate predominantly trench-normal compression along the southern arc and a shift toward trench-parallel stress in the Sunda Strait region (**Capitanio et al., 2025; Shamim et al., 2019**).

Our analysis tests the robustness of this pattern against the regional fault map and uses it to interpret how stress may be partitioned, drawing on the framework used by **Zuhair** (**2022**).

3.4. Gravity Data and Processing

Gravity data in this study were sourced mainly from satellite-derived global gravity models, using the TOPEX/POSEIDON-based gravity dataset (TOPEX2014) distributed by Scripps Institution of Oceanography (**Sandwell et al., 2014**). This dataset provides Free-Air Anomaly (FAA) values together with satellite-derived topography/bathymetry, making it well-suited for regional-scale tectonic analysis. Numerous studies have shown that satellite complex settings, including subduction margins, are especially prevalent in regions where terrestrial gravity measurements are limited or spatially inconsistent (**Förste et al., 2014; Hirt et al., 2011; Sandwell et al., 2014; Wu et al., 2021**).

3.4.1. Pre-processing and Free-Air Anomaly

The TOPEX gravity data were obtained in gridded format and imported into Oasis montaj™ (Geosoft) for subsequent processing and analysis. The dataset provides Free-Air Anomaly (FAA) values referenced to mean sea level, which account for elevation effects but do not yet correct for the mass between the observation point and the datum. FAA serves as the starting point for Bouguer and terrain corrections.

3.4.2. Simple Bouguer Anomaly Calculation

The Simple Bouguer Anomaly (SBA) was calculated from the FAA by applying a Bouguer slab correction using an assumed crustal density. A reduced density of 2.67 g/cm³ was adopted for onshore regions, corresponding to the average density of continental upper crust and commonly used in regional gravity studies (**Hinze, 2003**). The selected density is suitable for Java because the island is largely undelain by continental and volcanic-arc rocks. In offshore regions, the water layer is already accounted for through the FAA-based Bouguer correction and terrain correction, eliminating the need to apply a separate oceanic reduction density during SBA computation.

3.4.3. Terrain Correction

Terrain corrections were applied to remove the gravitational effect of topography and bathymetry, using both local and regional DEMs. A high-resolution DEM was used for near-field correction, while a coarser regional DEM accounted for far-field terrain contributions. Calculations were performed in Oasis montaj™ using standard ring-zone or prism-based algorithms to properly correct for mass surpluses and deficits in areas of rugged relief (**Hinze, 2003**).

3.4.4. Complete Bouguer Anomaly (CBA)

The Complete Bouguer anomaly (CBA) was calculated by combining the free-air anomaly (FAA) with the Bouguer slab, terrain, and elevation corrections. After removing the gravitational contributions of topography and elevation, the resulting CBA highlights subsurface density contrasts and therefore provides a solid basis for interpreting crustal to lithospheric scale structures. The final CBA grid was resampled to an approximate resolution of 5 × 5 km, which is sufficient to capture regional tectonic patterns while limiting the amplification of high-frequency noise that commonly affects satellite gravity products.

3.4.5. Spectral Analysis and Regional–Residual Separation

We applied spectral filtering to the CBA grid to separate long-wavelength lithospheric contributions from

short-wavelength crustal effects, using the Radially Averaged Power Spectrum (RAPS) method. The RAPS results were used to highlight dominant wavelengths and to estimate depth intervals for key density interfaces, including the Moho. We decomposed the anomaly field into regional and residual components using wavelength-based filters in Oasis montaj™. Such an approach is widely used in subduction and arc-related settings to discriminate signals linked to slab geometry and crustal thickness from anomalies produced by shallow structures and volcanic sources (**Banerjee & SubbaRao, 2020; Roy et al., 2025**).

3.5. Moho Depth Estimation Using the RAPS Method

Moho depth was estimated using the Radially Averaged Power Spectrum (RAPS) method applied to the Complete Bouguer Anomaly, following established spectral analysis procedures (**Eshagh et al., 2016; Hanif et al., 2024; Karner & Watts, 1983; Tselentis et al., 1988**).

The study area was divided into 1° × 1° windows, each exceeding six times the expected Moho depth to ensure spectral reliability. For each window, a 2-D Fast Fourier Transform (FFT) was applied, and the logarithmic power spectrum (- 10 to 10) was plotted against radial wavenumber (0 to 10.000).

Uncertainty estimates were obtained through linear regression analysis. The resulting Moho depths were validated against receiver function studies and global crustal models (**Bahri et al., 2021; Laske et al., 2013; Syuhada & Anggono, 2016**), confirming consistency within the expected uncertainty range.

3.6. Seismic Reflection Data and Interpretation

The two-dimensional seismic reflection data used in this study comprise archived (secondary) profiles obtained from the Data Center of Indonesia's Ministry of Energy and Mineral Resources (ESDM). These lines were originally collected for regional geological mapping and hydrocarbon exploration and were provided in SEG-Y format, including both offshore (marine) and onshore profiles. No new seismic surveys were conducted for this work; instead, we re-interpret the existing profiles within an integrated tectonic framework.

The seismic reflection dataset includes four regional lines that traverse southern, central, and northern Java: D–D′ (~220 km), E–E′ (~60 km), F–F′ (~30 km), and G–G′ (~160 km). Together, these profiles span an area of roughly 109°E–112°E longitude and 5.3°S–9.7°S latitude, providing across-margin transects from the forearc and volcanic arc into the back-arc domain. Although these lines have been referenced in earlier regional work mainly for descriptive earthquake seismicity and stress-orientation constraints, to better define structural geometry and depth relationships.

3.6.1. Data Processing Level and Limitations

The seismic profiles were provided by ESDM in a pre-processed form, having undergone routine processing steps including geometry assignment, deconvolution, velocity analysis, normal moveout (NMO), stacking, and time-domain migration. Based on the accompanying metadata and documentation, the migration is interpreted as Post-Stack Time Migration (PSTM). Pre-Stack Depth Migration products were not available, and no additional reprocessing was carried out in this study. Accordingly, all interpretations are made in the time domain (two-way travel time, TWT), and we do not attempt depth conversion because a consistent velocity model is not available.

Using PSTM data means that reflector geometry is generally dependable at a regional scale, but local positioning can be influenced by velocity heterogeneity, especially beneath volcanic terrains and structurally complex zones. We explicitly account for these uncertainties when assessing fault continuity, reflector configuration, and overall structural style (**Sherif & Geldart, 1995; Yilmaz, 2001**).

3.6.2. Seismic Interpretation Workflow

We interpreted the pre-processed PSTM 2D seismic profiles in Petrel™ (Schlumberger). The interpretation relied mainly on reflector geometry and continuity, complemented by fault-related reflector responses and regional geological context.

The workflow included:

- Horizon picking on the most laterally continuous reflectors with consistent phase/amplitude, used as seismic markers for structural analysis (not definitive formation tops due to the absence of well ties).
- Fault mapping based on reflector offsets, truncations/terminations, abrupt dip changes, and localized loss of continuity. Interpretations were retained only where these indicators were coherent across adjacent reflectors.
- Structural classification (thrust, normal, strike-slip) where reflector patterns and kinematic indicators were consistent with the regional tectonic setting.

Structural forms were defined explicitly from reflector patterns. Convex-upward and concave-downward geometries were interpreted where reflectors show systematic arching or sagging across multiple horizons, reducing the risk of noise- or migration-related artifacts (**Sherif & Geldart, 1995; Yilmaz, 2001**). Locally, Y-shaped patterns were interpreted where reflector packages diverge upward adjacent to fault zones, consistent with fault-propagation folding or flower-structure style deformation in compressional to transpressional settings (**Harding & Lowell, 1979; Suppe, 1983**).

Amplitude loss or chaotic reflections were treated cautiously, especially beneath volcanic/volcaniclastic

segments, and interpretations were limited to areas where reflector geometry remained traceable. Seismic results were also cross-checked against mapped surface faults and published tectonic frameworks for Java to strengthen geological consistency (**Hall & Smyth, 2008; Widiyantoro et al., 2020**).

3.7. Integration of Geophysical Methods

The integration of different geophysical methods in this study was designed to link observations across multiple spatial scales, from deep slab geometry to upper-plate deformation, and to reduce non-uniqueness inherent in single-dataset interpretations. Each dataset provides complementary constraints on the tectonic system beneath southern Java, and integration was achieved through spatial correlation, cross-validation, and hierarchical interpretation.

Seismicity data and focal mechanism solutions provide direct constraints on the geometry of the subducting slab, depth distribution of earthquakes, and faulting styles. These data were first analyzed independently to delineate the Wadati–Benioff zone, identify depth-dependent variations in seismicity density, and characterize fault kinematics. Event-based stress orientations derived from focal mechanisms were then used to infer the regional stress regime and to evaluate the kinematic consistency between stress directions and mapped fault trends.

Gravity data supply independent constraints on crustal density variations and crustal thickness that cannot be resolved from seismicity alone. Complete Bouguer Anomaly maps and their regional–residual separation were spatially compared with seismicity patterns and stress orientations to assess whether zones of earthquake clustering or reduced seismicity coincide with major density contrasts. Spectral analysis of gravity data using the Radially Averaged Power Spectrum (RAPS) method provided estimates of Moho depth, which were used to anchor the depth extent of tectonic features inferred from seismic observations.

The 2D seismic reflection profiles were treated as depth-constrained structural benchmarks to check and improve interpretations based on seismicity and gravity. Fault geometries and reflector breaks mapped on the seismic sections were evaluated against surface gravity gradients, focal-mechanism patterns, and stress-orientation data to assess their consistency and tectonic significance.

Integration in this study was therefore achieved not through mathematical dataset fusion, but through iterative spatial comparison and mechanical consistency checks across seismicity, stress, gravity, Moho-depth estimates, and seismic reflection interpretations. By relying on multiple independent lines of evidence, this workflow strengthens the robustness of the structural interpretation and provides a coherent tectonic framework for discussing slab segmentation, crustal architecture, and active faulting beneath southern Java.

4. Results

4.1. Seismicity Distribution and Cross-Sectional Patterns

The seismicity dataset used in this study includes 48.825 earthquakes recorded between 2000 and 2023, whith magnitudes spanning Mb 2.7-7.8 and hypocentral depths ranging from 10 to 600 km. All events were obtained from the USGS earthquake catalog (**USGS, 2023**). No additional relocation (e.g. double-difference or regional network relocation) was applied; therefore, the analysis relies on catalog locations as provided. This limitation is considered when interpreting fine-scale features in the cross sections.

Spatially, earthquake epicenters define a continuous seismic belt parallel to the Sunda–Java Trench, extending landward beneath Java (see **Figure 1**). Hypocentral depths increase systematically from shallow earthquakes (<30 km) near the trench, through intermediate-depth events (70–200 km) beneath the volcanic arc, to deep-focus earthquakes (200–400 km) beneath central Java, and very deep events (>600 km) north of the Java Sea. The progression of earthquake depths outlines a clear, northward-dipping Wadati-Benioff zone, in line with the subducting Indo-Australian Plate beneath Java (**Hutchings & Mooney, 2021; Isacks, 1971**).

The shallowest group dominates; 26,19 earthquakes are recorded at 10-30 km, pointing to brittle deformation in the upper crust and along the shallow plate interface. At intermediate depths, 10,856 events occur between 40 and 90 km, capturing the shift from deformation in the overriding plate to processes within or near the descending slab. A total of 9,583 earthquakes were recorded between 100 and 300 km, corresponding to deformation within the subducting slab, while 2,189 deep-focus events occurred at depths of 300–670 km, indicating continued seismic activity within the deeper slab.

Magnitude-frequency statistics indicate that seismicity in the region is dominated by low- to moderate-magnitude earthquakes. Events with magnitudes Mb 2.7–4.2 total 13,281, while Mb 4.2–4.5 earthquakes are the most frequent (16,723 events). Earthquakes with magnitudes Mb 4.5–4.9 number 12,808, followed by 4,438 events in the Mb 4.9–5.4 range. Larger events are comparatively rare, with 1,286 earthquakes between Mb 5.4 and 6.1, and 289 earthquakes exceeding Mb 6.1.

To examine along-strike variations in seismicity, three trench-perpendicular cross sections (A–A′, B–B′, and C–C′) were constructed using identical lateral windows and depth scaling (see **Figure 1**). The location of the Sunda–Java Trench and slab geometry used as reference were adapted from the Seismicity of Indonesia and Java

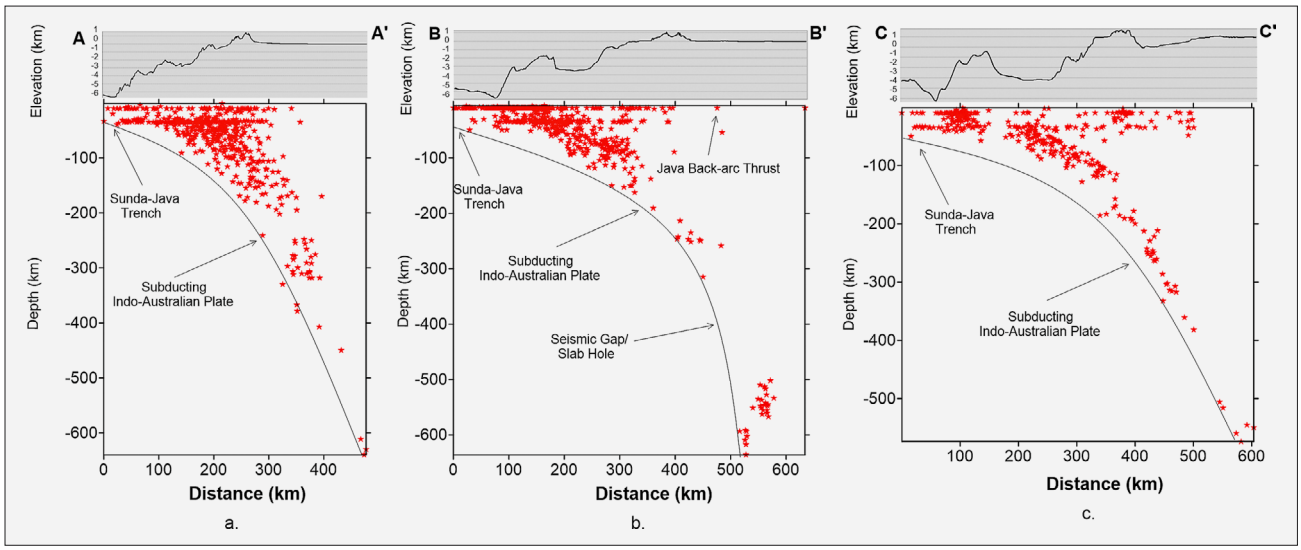


Figure 2: Trench-perpendicular earthquake cross-sections across Java showing hypocenter distribution with depth. (a) A–A′ (western Java), (b) B–B′ (central Java), and (c) C–C′ (eastern Java). Earthquake hypocenters (**USGS, 2023**) are projected onto each profile within the same corridor width and plotted by depth (km). The red star symbols indicate earthquake occurrences (hypocenters) along the section. The black curved line represents the reference geometry of the subducting Indo-Australian slab (subduction interface) used to guide the cross-sectional comparison. The location of each profile is shown in **Figure 1**.

Sumatra segments of the Sunda Trench (**Hutchings & Mooney, 2021; Lemenkova, 2020**), combined with global bathymetry and topography datasets (e.g. ETOPO1, BATHNAS, DEMNAS). The cross-sections were generated by projecting earthquake hypocenters onto each profile within a consistent corridor width.

The western (A–A′) and eastern (C–C′) sections display relatively continuous seismicity from shallow to intermediate depths, with earthquakes distributed along the downgoing slab without pronounced gaps (see **Figure 2a, c**). In contrast, the central Java section (B–B′) exhibits a notable reduction in earthquake occurrence at depths of approximately 80–180 km, while seismicity is present both above and below this interval (see **Figure 2b**). This feature is identified purely based on the spatial distribution of earthquake hypocenters within the catalog and is not constrained by focal mechanism inversion, coupling estimates, or geodetic parameters.

In cross-section A–A′ (see **Figure 2a**), seismicity is concentrated near the trench at depths <50 km, with deeper earthquakes delineating the slab to depths exceeding 200 km. In cross-section B–B′ (see **Figure 2b**), shallow seismicity (<50 km) is again prominent near the trench, and intermediate-to-deep earthquakes outline the slab geometry; however, a relative paucity of events is observed at depths of approximately 400–500 km. This zone is referred to here as an observational seismic gap, defined strictly by reduced earthquake density in the catalog. Additionally, shallow earthquakes at depths <30 km beneath northern Java spatially coincide with previously reported activity along the Java Back-Arc Thrust. In cross-section C–C′ (see **Figure 2c**), shallow trench-related seismicity and deeper slab earthquakes extending to approximately 300 km depth are observed, without a comparable reduction in event density at greater depths.

4.2. Earthquake Focal Mechanism Characteristics

A total of 534 focal mechanism solutions were analyzed in this study, obtained from the GEOFON Program (**Förste et al., 2014; Helmholtz-Zentrum Potsdam, 2024**). The dataset covers 2011-2023 and matches the spatial footprint of the seismicity analysis, ensuring that earthquake distributions and source-mechanism interpretations are directly comparable. The events analyzed span Mb 4.0-7.0, a range that is generally sufficient to yield stable moment-tensor solutions and reliable fault-plane characterization.

Focal mechanisms reveal three main faulting modes: normal, reverse (thrust), and strike-slip, underscoring a heterogeneous stress field along the Sunda-Java margin. Strike-slip solutions include both dextral and sinistral motion, suggesting localized shear deformation in the upper plate and occasionally within the subducting slab. The spatial distribution of mechanisms indicates marked tectonic segmentation (see **Figure 1**). Normal faulting is prevalent along the subduction interface and within the downgoing slab, especially at intermediate-deep depths, consistent with slab bending and extensional stresses related to slab pull (**Houston, 2007; Isacks, 1971**). In contrast, reverse mechanisms dominate south of Java near the trench and forearc, reflecting compressional stresses associated with convergence and megathrust coupling.

Onshore Java exhibits a mixture of reverse and strike-slip mechanisms, with notable right-lateral strike-slip events. This pattern suggests that compression and shear

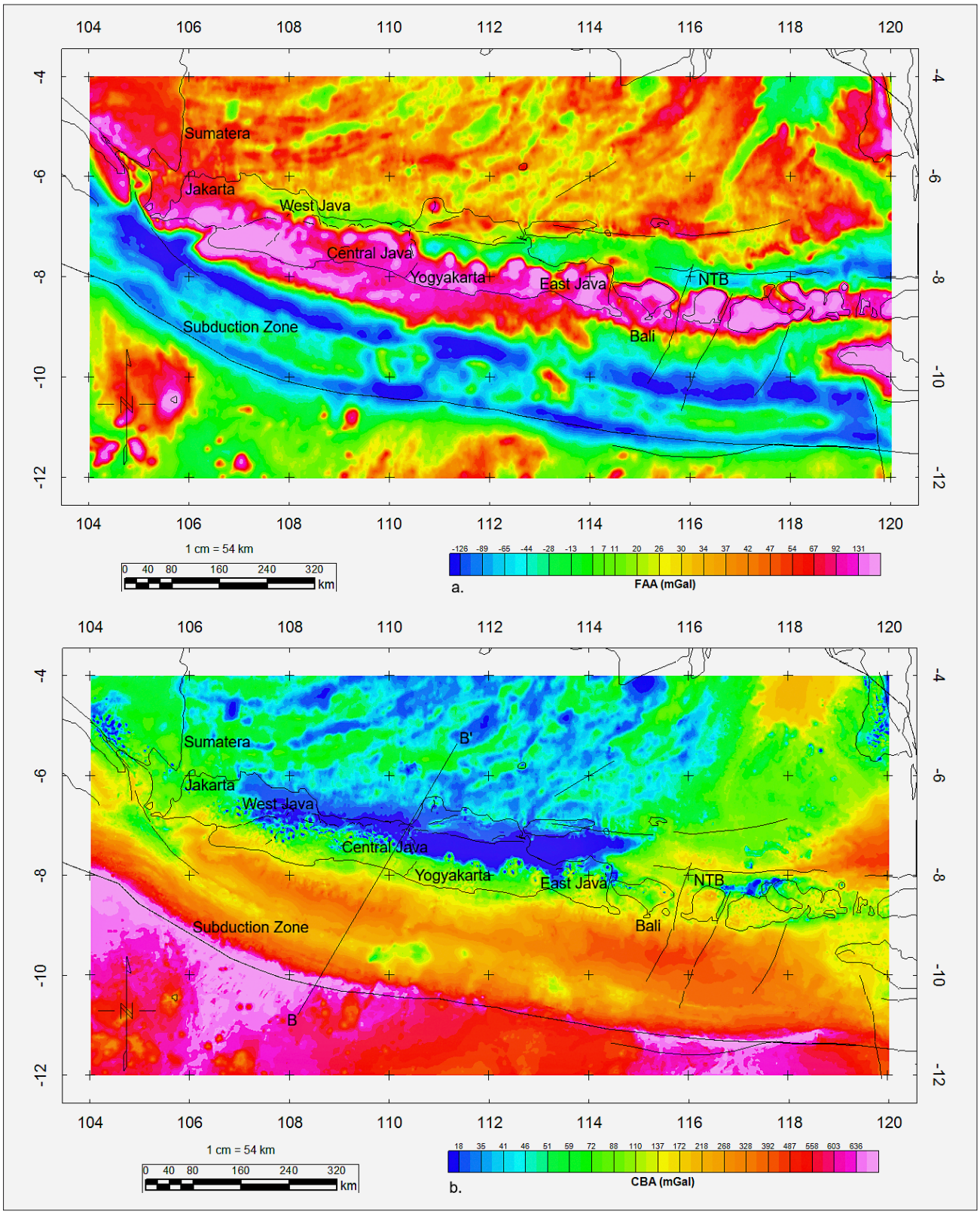


Figure 3: Gravity anomaly maps of the Southern Sunda Arc within the study area: (a) Free-Air Anomaly (FAA) and (b) Complete Bouguer Anomaly (CBA). The black line B–B′ marks the location of the gravity profile extracted from the CBA grid and used for 2-D forward gravity modelling (see **Figure 13b**).

act together within the upper plate, in line with the influence of the Java Back-Arc Thrust and related strike-slip fault systems (**Patria & Aulia Nur, 2020; Supendi et al., 2018**). North of Java, beneath the Java Sea, deep earthquakes are dominated by normal-fault mechanisms, which are typical of extension in the deeper slab and are

often attributed to slab unbending or gravitational descent at depth (**Scholz, 2002**).

4.3. Stress Orientation Results

We derived stress orientations from individual focal mechanisms and supplemented them with regional stress information from the World Stress Map (**Heidbach et al., 2010, 2018**). The dataset is restricted to 106°E–114°E and 7°S–10°S, ensuring consistency with the study area used for the seismicity, gravity, and seismic reflection components.

Figure 1 presents stress orientations in an event-based form rather than as an interpolated or zonal field. This choice preserves local heterogeneity and avoids artifacts that can occur when interpolating over unevenly distributed seismicity, common in subduction zones, where events cluster along distinct structures (**Michael, 1987**). Interpolation can artificially smooth or connect regions with sparse data, potentially obscuring meaningful variations tied to slab geometry, fault segmentation, or rheological contrasts. Event-based orientations, by comparison, provide direct constraints on the stress regime at the earthquake source locations, which is well-suited to a complex margin like Sunda-Java.

The stress-orientation analysis is not intended to introduce a new regional stress model. Instead, it serves as a kinematic framework for interpreting the patterns observed in seismicity, gravity anomalies, and subsurface structure. In practice, the stress map is used to (i) test whether the observed faulting styles and apparent seismic gaps are compatible with the inferred stress regime, and (ii) examine how well stress orientations align with structural trends derived from gravity gradients and seismic reflection profiles.

As illustrated in **Figure 1**, the stress orientations include both trench-parallel and trench-normal components, consistent with the combined effects of plate convergence, slab bending, and deformation within the upper plate across the forearc-arc-back-arc system. Along the subduction zone, the pattern is dominated by normal-faulting (NF) indicators (red), implying extension within parts of the downgoing Indo-Australian slab and commonly linked to slab bending and intraslab deformation (**Isacks, 1971**). South of Java, strike-slip (SS) indicators (purple) become more common, pointing to localized shear partitioning within the forearc and overriding plate, potentially promoted by oblique convergence and along-arc changes in coupling. Thrust-faulting (TF) indicators (brown) are less frequent and occur mainly along the southern Java margin and toward the Nusa Tenggara sector, consistent with compression associated with interplate coupling and bar-arc shortening.

We compare stress orientations spatially with (a) zones of reduced seismicity in the B-B' cross-section, (b) gravity-derived density contrasts and Moho-depth estimates, and (c) faults mapped from seismic reflection profiles. This comparison tests whether reduced seismicity of distinctive gravity patterns are associated with changes in stress regime, strengthening the integrated tectonic interpretation. The stress map, therefore, acts as an independent kinematic constraint that complements, rather than duplicates, interpretations from seismicity and gravity (**Heidbach et al., 2018**).

4.4. Gravity Anomaly Results

Gravity results presented in this study are based on satellite-derived gravity data obtained exclusively from the TOPEX/POSEIDON global gravity model (**Sandwell et al., 2014**). No terrestrial or shipborne gravity measurements were incorporated. The gravity grid covers the same spatial extent as the seismicity analysis, approximately 106°E–114°E longitude and 7°S–10°S latitude, and is represented at a uniform spatial resolution of ~5 × 5 km.

The Free-Air Anomaly (FAA) map (see **Figure 3a**) shows values ranging from approximately –89 to –44 mGal along the southern offshore region adjacent to the Sunda–Java Trench. On the islands of Java, Bali, and West Nusa Tenggara, FAA values are generally higher, reaching approximately 54 to 131 mGal and outlining wide domains of positive gravity anomalies.

The CBA map (see **Figure 3b**) ranges from about -120 mGal to 140 mGal. High values form a continuous, trench-parallel belt in the southern offshore area, whereas anomalies decrease landward across the forearc and volcanic arc. Central Java is marked by broad, lower-anomaly zones that extend along strike, followed by a renewed increase toward northern Java that produces a prominent positive anomaly domain.

Spectral decomposition divides the CBA into regional and residual fields (see **Figures 5-6**). The regional anomaly represents the dominant long-wavelength signal and emphasizes across-arc contrasts between the southern offshore sector, central Java, and northern Java. The residual anomaly highlights shorter-wavelength features, appearing as localized positive and negative anomalies superimposed on the regional background across both land and offshore regions.

4.5. Moho Depth Estimates Based on RAPS and Gravity Decomposition

Figure 4 presents the Radially Averaged Power Spectrum (RAPS) calculated from the Complete Bouguer Anomaly (CBA) field. RAPS evaluates how gravity-anomaly power is distributed across spatial frequencies; changes in the spectral slope can therefore be used to infer the depths of major density boundaries. The spectrum shows four clear linear segments, interpreted to represent four depth levels. The corresponding depths are 94.5 km, 36.2 km, 14.5 km, and 5.2 km, which we interpret as the deepest density interface, the Moho, the Conrad discontinuity, and the basement, respectively.

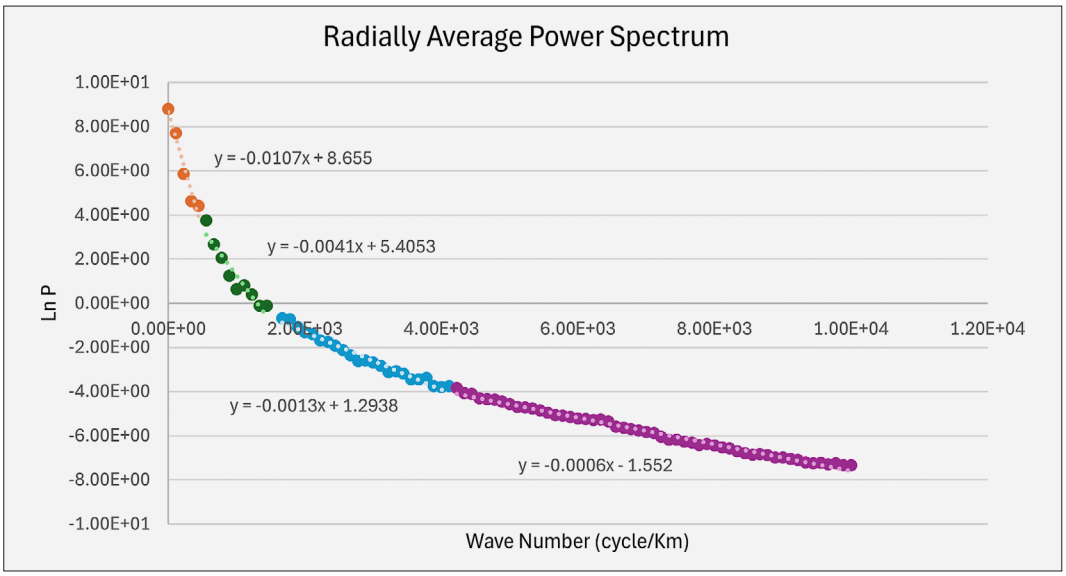


Figure 4: Radially averaged power spectrum (RAPS) derived from the Bouguer anomaly, with spectral segments interpreted as the subduction zone (orange), Moho (green), Conrad discontinuity (blue), and basement (purple).

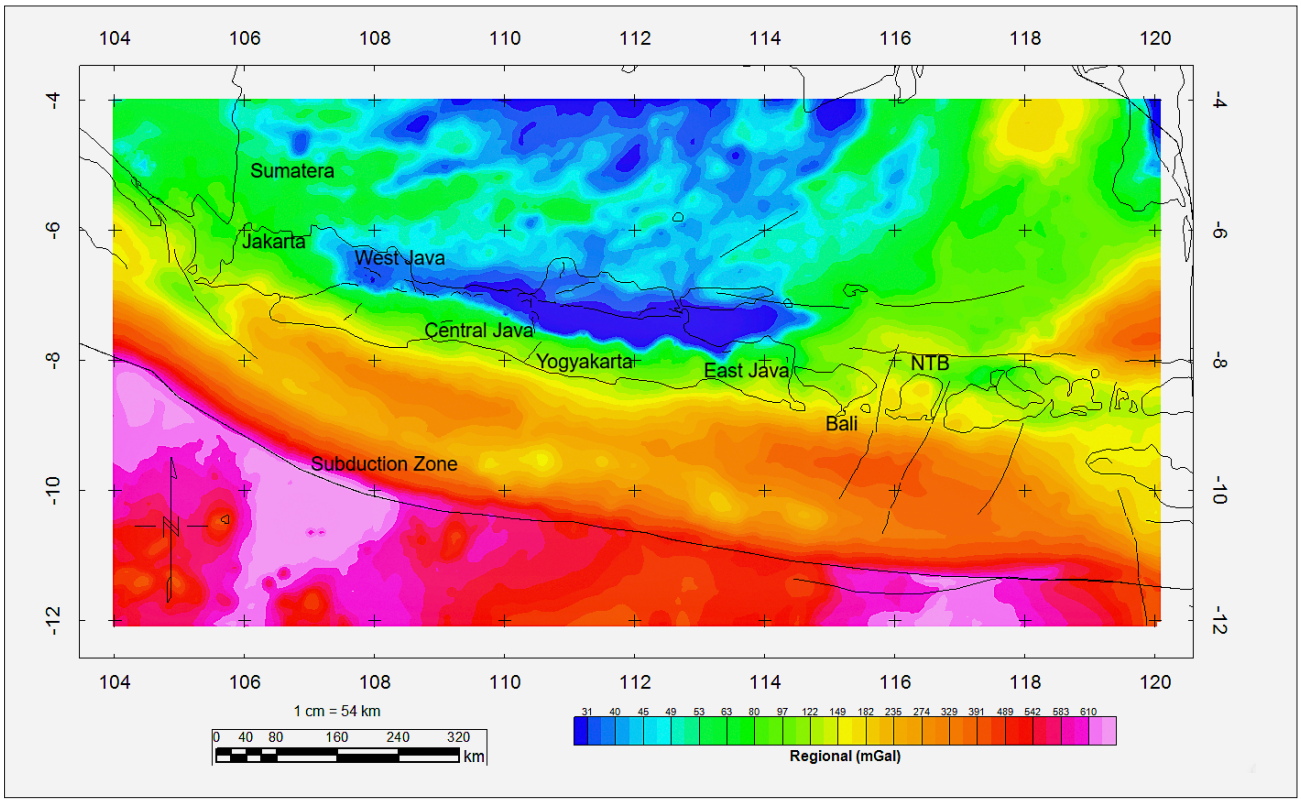


Figure 5: Regional Bouguer Anomaly of Southern Sunda Arc

Moho depths inferred from the long-wavelength gravity component vary noticeably across the study area, highlighting clear lateral differences in crustal structure. The calculated Moho depths range from approximately ~30 km beneath northern Java to ~55 km beneath central and southern Java (see **Figure 11**). The observed distribution suggests regional, systematic changes in crustal thickness as resolved from the gravity spectrum.

RAPS is commonly applied in regional gravity analysis to discriminate deep lithospheric interfaces from shallow crustal features, relying on the principle that longer wavelenghths by near-surface structures (**Hanif et al., 2024; Roy et al., 2023; Tselentis et al., 1988; Xuan & Jin, 2022**).

In **Figure 5**, we display the regional field obtained by decomposing the CBA with the RAPS method. Since the

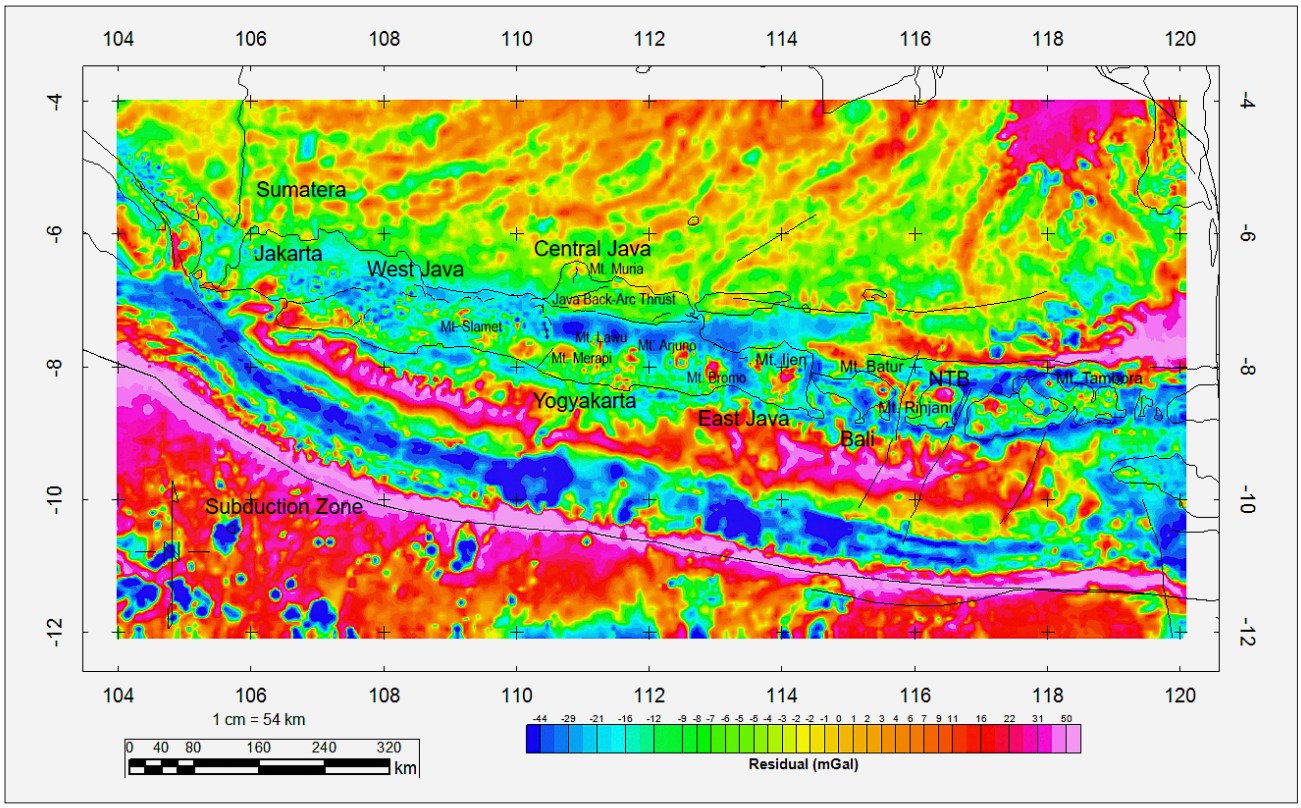


Figure 6: Residual Bouguer Anomaly of Southern Sunda Arc

regional component is defined by the long-wavelength part of the spectrum, it brings out the large-scale gravity patterns across the Sunda-Java margin. These patterns form clear spatial contrasts that track the major tectonic domains.

The regional field shows a clear three-part pattern. The southern offshore zone, parallel to the Sunda-Java Trench, exhibits the highest values (895-610 mGal). Northern Java stands out with much lower anomalies (31-40 mGal). Central Java sits in between, with moderate values of 149-329 mGal that extend laterally and act as a continuous bridge between the southern offshore and northern Java domains. These first-order regional patterns are consistent with gravity responses typically observed across subduction-related forearc, arc, and back-arc systems in previous regional studies (**Green et al., 1981; Sandwell et al., 2014; Syuhada & Anggono, 2016**).

Figure 6 shows the residual anomaly extracted from the CBA after removal of the regional component using RAPS-based wavelength thresholds. The residual field highlights short-wavelength features, expressed as localized gravity highs and lows. Residual values of 50 mGal appear along the southern margin, while minima down to -44 mGal occur within parts of the Java Basin. A further set of localized positive residual anomalies (31 mGal) is observed in the frontal forearc.

Several volcanic centers, including Mount Slamet, Merapi, Bromo, Batur, and Rinjani, are expressed as localized positive residual anomalies, indicating distinct short-wavelength gravity signatures within the arc region. Such expressions of volcanic systems in residual gravity fields have been widely reported in arc-related gravity studies, where residual anomalies are used to isolate near-surface and upper-crustal density contrasts from deeper lithospheric signals (**Banerjee & Subba-Rao, 2020; Handayani et al., 2022; Hanif et al., 2024**).

In the northern Java area, the residual gravity field also shows pronounced lateral density contrasts aligned along strike. Similar residual anomaly patterns along the northern Java margin have been documented in previous gravity-based regional models, which describe strong short-wavelength variations superimposed on a broader regional field (**Green et al., 1981; Handayani et al., 2022**). The residual anomalies identified here provide a detailed representation of short-wavelength gravity variability that complements the regional anomaly field derived from the RAPS-based separation.

4.6. Seismic Reflection Profile Observations

Three 2D seismic reflection profiles were examined in this study (D–D′, E–E′, F–F′, and G–G′), provided in pre-processed, time-migrated (PSTM) format. The line lengths are approximately 225 km (D–D′), 48 km (E–E′), 30 km (F–F′), and 163 km (G–G′).

The profiles show intervals of laterally continuous reflectors alternating with zones of reduced continuity and disrupted reflection character. Reflector terminations

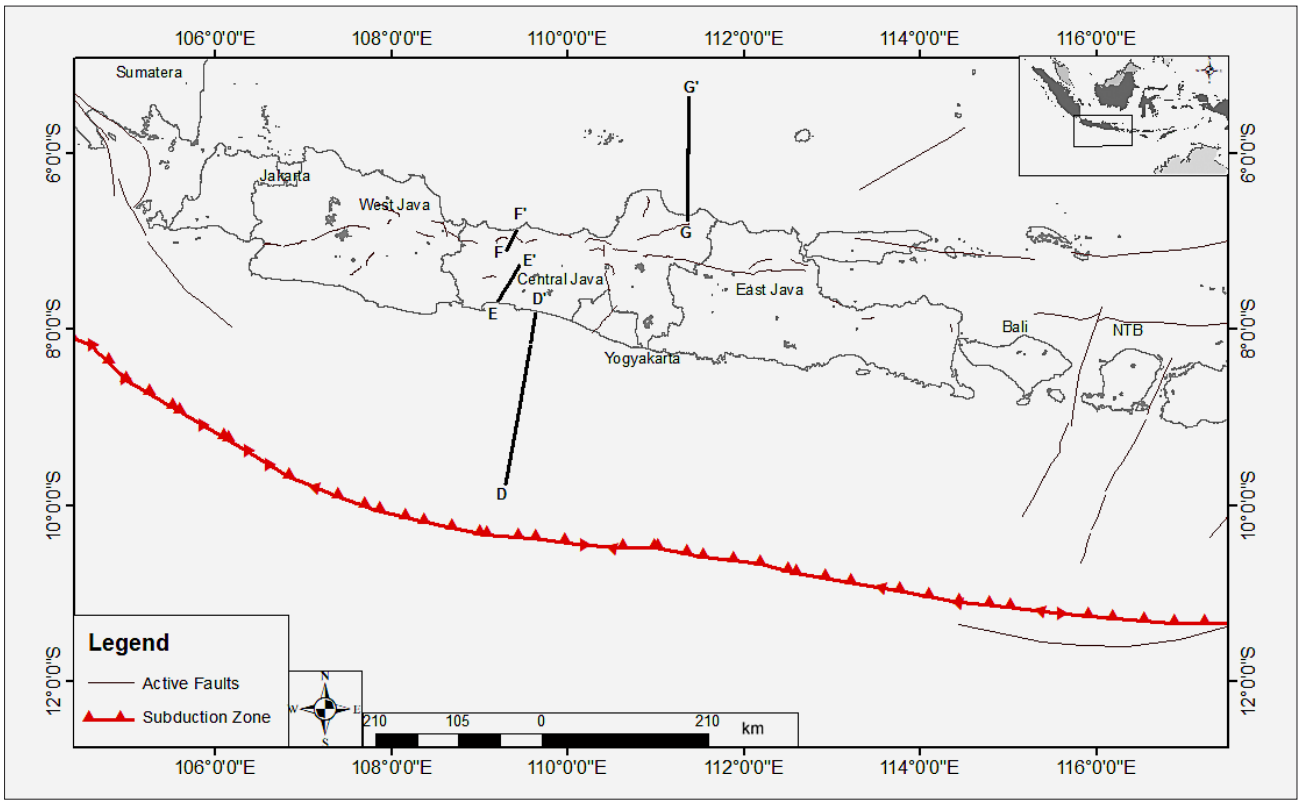


Figure 7: Basemap showing the distribution of 2D seismic reflection profiles within the study area. Black lines indicate the locations of the seismic reflection lines used in this study. The red line marks the axis of the Sunda–Java subduction zone, while brown lines denote mapped active faults based on regional tectonic compilations. This map provides the spatial context for the seismic sections presented and interpreted in subsequent figures.

and local loss of coherence are particularly evident beneath parts of central Java. In subvolcanic segments, the reflection character becomes more scattered, with locally incoherent events.

Several fault-like discontinuities are recognized based on reflector offsets, truncations/terminations, and abrupt changes in reflector continuity. No depth conversion was undertaken; therefore, all seismic observations and interpreted geometries are reported in two-way travel time (TWT).

On the seismic sections, two main horizons were interpreted for structural analysis, displayed as an upper horizon (blue) and a lower horizon (green). These horizons were selected through horizon picking of the most laterally continuous and high-amplitude reflectors, which can be traced consistently across segments with relatively good data quality. Since no well data, checkshot surveys, or velocity logs are available, the stratigraphic interpretation is considered tentative and is based on reflector characteristics and comparison with established regional stratigraphic frameworks reported in the literature.

Based on this correlation, the upper horizon (blue) is tentatively associated with the Cisubuh Formation, whereas the lower horizon (green) is correlated with the Upper Cibulakan Formation. Previous studies describe the Cisubuh Formation as a shallow sedimentary unit composed of gravel in its upper part, with a middle interval characterized by alternating sandstone, siltstone, and claystone, and a lower interval dominated by claystone and shale with thin interbeds of sandstone and siltstone (**Aribowo et al., 2022; Exploration Unit EP III, 1990; Herninda & Mohamad, 2021**).

The Upper Cibulakan Formation is reported to have been deposited at depths of approximately 1550–2300 m and consists of alternating sandstone, limestone, shale, and siltstone, with an age ranging from the Early to Middle Miocene (**Exploration Unit EP III, 1990**). This formation is typically subdivided into several units, namely the Massive Unit, the Main Unit, containing interbedded limestone (**Jambak et al., 2015**).

Since we do not have direct well ties, the picked horizons are treated as seismic markers to guide structural interpretation, not as strict formation boundaries.

The D-D' profile across southern offshore Java (see **Figure 8**) captures many of the features expected in an active subduction margin. At the trenchward edge, the section images a clear accretionary prism, seen as imbricated packages of discontinuous reflectors with changing dips. Moving landward, a forearc basin appears roughly 50-140 km from the trench, with the main reflection packages occurring at about 3000-5000 ms TWT.

On the seaward side, the basin is limited by an outer forearc high, expressed by uplifted and deformed reflec-

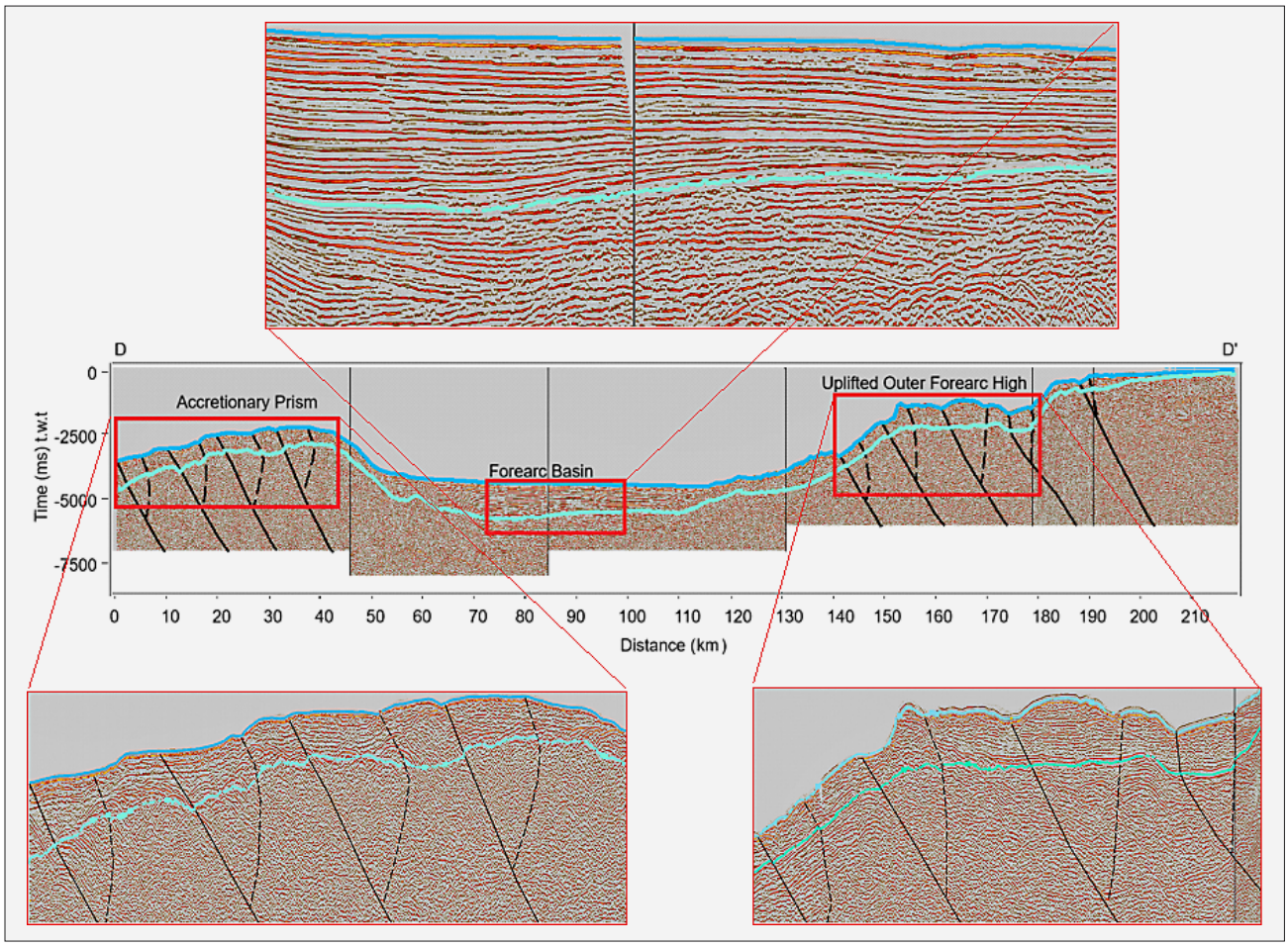


Figure 8: 2D Seismic Reflection Profile Line D-D'

tors. Inside the basin, strata systematically dip landward and locally show onlap onto the outer forearc high. These geometries suggest a relatively narrow basin, confined by uplifted structural highs along its seaward margin.

Overall, the D-D' profile can be divided into three main domains: (1) a trenchward accretionary prism, (2) a forearc basin dominated by layered, tilted reflectors, and (3) an uplifted outer forearc high. The configuration and seismic character of these domains agree with earlier interpretations of the erosional forearc margin offshore southern-central Java reported in regional studies (**Kopp et al., 2006; Patria & Aulia Nur, 2020**).

The E-E' line, situated south of Maunt Slamet (see **Figure 9**), images a shallow structural break interpreted as a thrust-related reflector offset between 7 and 22 km along the profile. It is expressed by reflector truncations and vertical displacements within the upper sedimentary sequence. This subsurface feature coincides with a subtle topographic rise (up to 400 m), forming a low-relief hill immediately south of the volcanic edifice. The spatial match between reflector offsets and surface relief suggests that near-surface deformation in this area is structurally controlled.

The F-F' profile across central Java near Mount Slamet (see **Figure 10**) shows a prominent thrust-related structure, marked by upward-stepping reflectors and systematic offsets. The thrust separates contrasting seismic packages and defines a clear upper-crustal structural boundary. In this section, the Mount Slamet volcanic edifice overlies deformed sedimentary reflectors, producing a hanging-wall geometry above the interpreted thrust zone.

In addition, the F–F′ section images shallow folded reflectors at approximately 1000–2000 ms two-way travel time (TWT). These folds exhibit laterally continuous, gently curved reflector geometries and are confined to the upper part of the seismic section. North of Mount Slamet, the seismic profile shows a series of imbricated reflector offsets forming a back-arc thrust belt, expressed by repeated reflector packages and localized uplifted blocks.

The overall reflector configuration and fault geometries observed in profiles E–E′ and F–F′ are consistent with previously reported seismic observations of back-arc thrust systems and upper-plate shortening in central Java, as documented in earlier regional studies (**Aribowo et al., 2022; Patria & Aulia Nur, 2020**).

The G–G′ seismic reflection profile, extending from Mount Muria toward the northern Java Sea (see **Figure 10**), images a thick, laterally continuous sedimentary

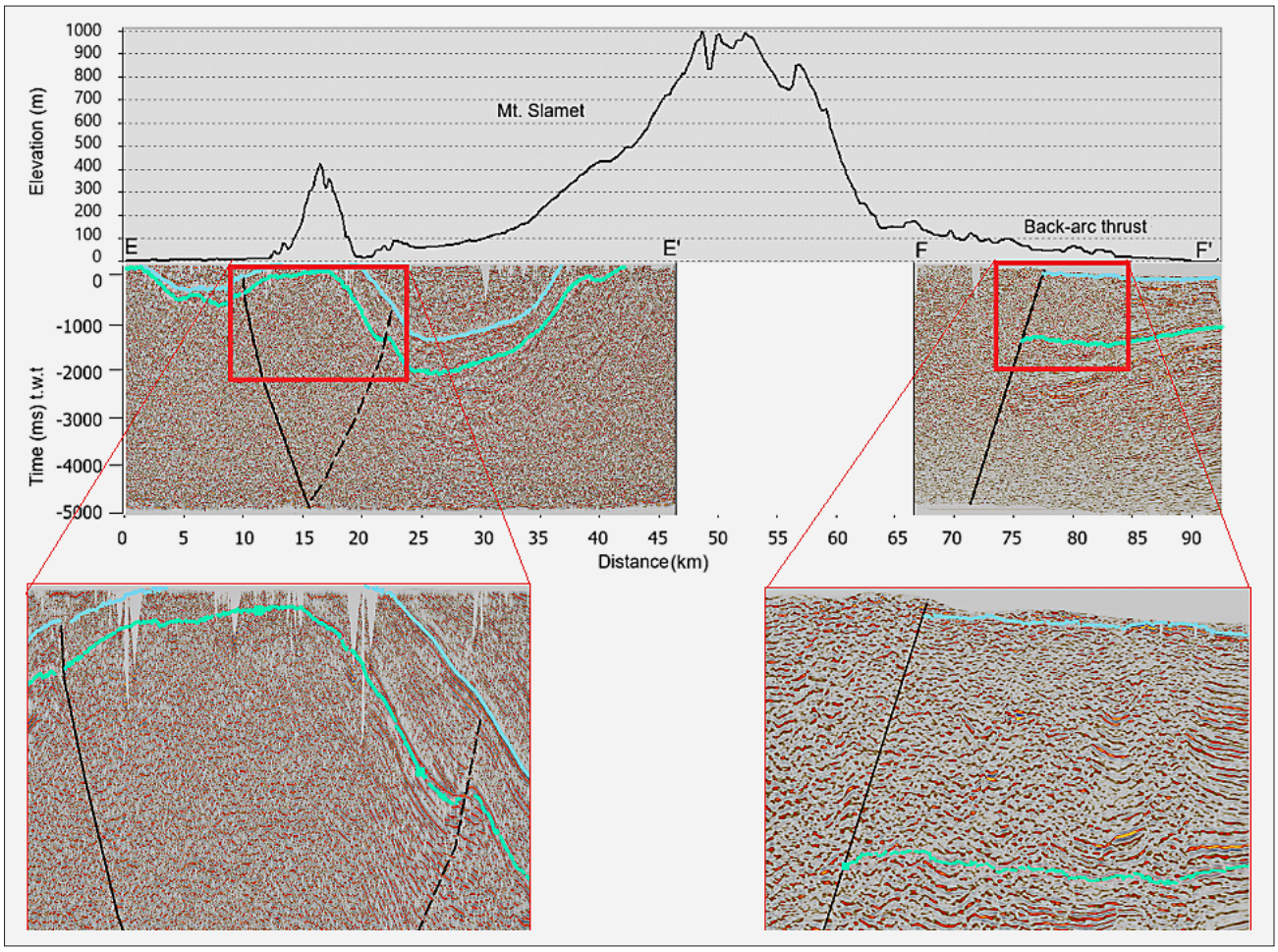


Figure 9: 2D Seismic Reflection Profile Line E-E' and Line F-F'

succession along most of the transect. Reflectors in this unit are mainly subhorizontal to gently dipping and remain laterally continuous over long distances, suggesting a regionally extensive depositional package beneath the northern Java margin. This reflection style is consistent with earlier seismic interpretations that describe the area as a transition between the volcanic arc and the northern back-arc basins (**Kopp et al., 2006; Patria & Aulia Nur, 2020**).

The G-G' section contains several fault-related breaks, seen as reflector offsets, step-like throws, and local loss of continuity within the upper-intermediate sedimentary sequence. The predominance of downthrown blocks and diverging reflectors supports an extensional (normal-fault) interpretation, while evidence for imbrication or compressional stacking is absent.

Thus, the G-G' architecture is defined by regionally continuous strata overprinted by localized extensional faulting. This structural style contrasts with the compressional geometries observed in profiles farther south. Independent observations show that the northern Java region is also characterized by deep-focus seismicity reaching depths of up to ~600 km (see **Figure 1**), where focal mechanism solutions are dominated by normal-faulting events, indicating an extensional stress regime at depth. While no direct causal relationship is inferred here, the spatial coincidence of extensional seismic structures and deep seismicity highlights the structural heterogeneity of the northern Java margin.

Overall, the interpreted 2D seismic reflection profiles provide independent geometric constraints on upper-crustal structure across Java, including the distribution and style of faulting (thrust- and normal-fault-related discontinuities), fold geometries, and the presence of laterally extensive sedimentary packages. These seismic observations complement the gravity results by providing a structural framework for evaluating spatial contrasts in the Complete Bouguer Anomaly and its regional–residual components, particularly where low-anomaly domains coincide with thick sedimentary successions and where localized residual anomalies coincide with uplifted or structurally disrupted zones. When considered together with the seismicity patterns, focal mechanisms, and stress-orientation indicators presented in this study, the seismic sections help establish a consistent dataset-level description of along-strike and across-arc variability in deformation from the forearc to the back-arc domains.

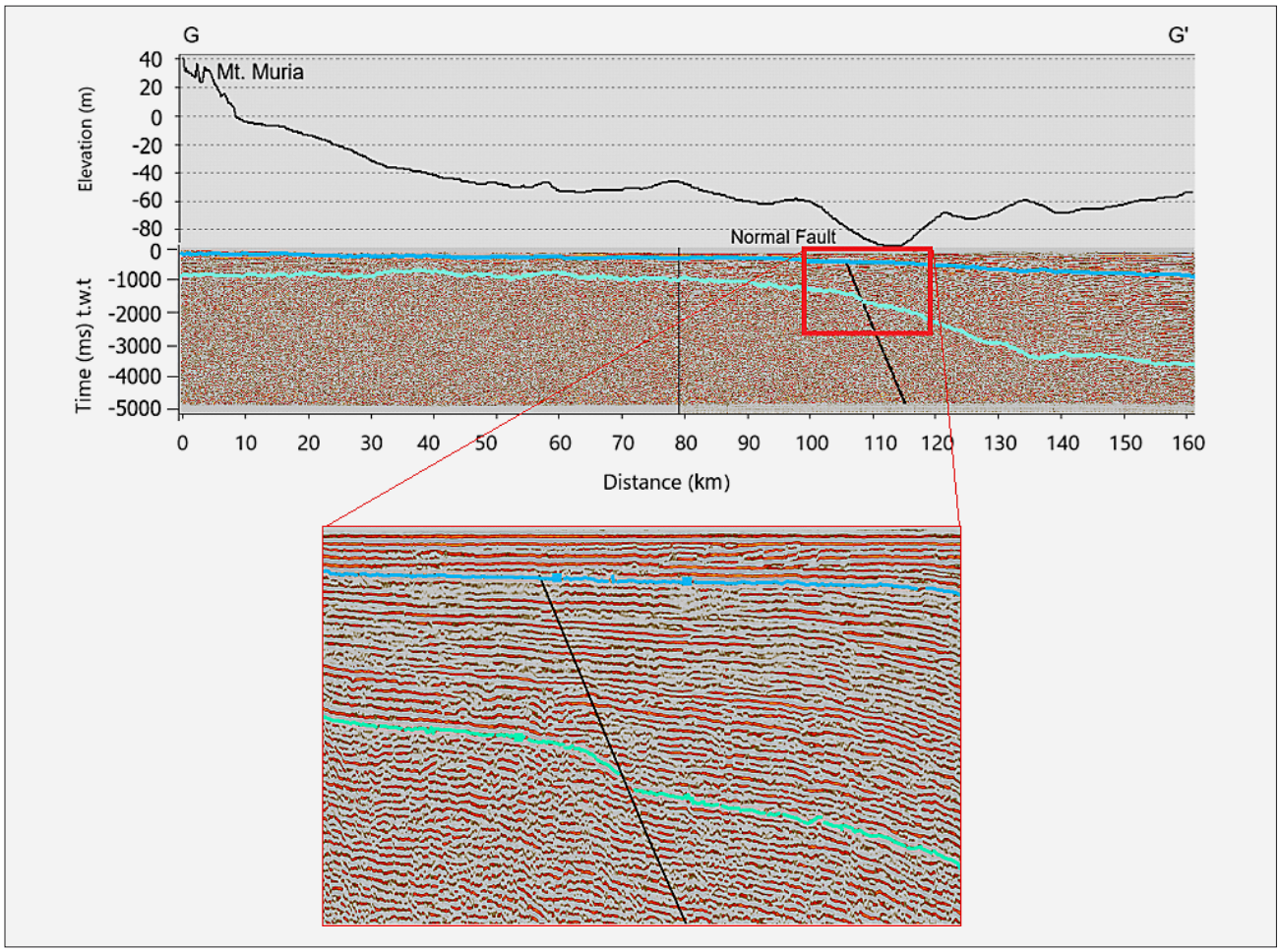


Figure 10: 2D Seismic Reflection Profile Line G-G'

5. Discussion

5.1. Implications of the Seismic Gap beneath Central Java

The relative reduction in seismicity observed along the B–B′ cross-section is identified from the USGS earthquake catalog, covering the period 2000–2023, which comprises 677 earthquake events with magnitudes ranging from Mb 3.5 to Mb 6.6 and hypocentral depths between 10 and 600 km. Within this dataset, a distinct decrease in earthquake occurrence is observed at intermediate to deep depths beneath central Java, while seismicity remains present both updip and downdip of this interval. In this study, the term' seismic gap' is used strictly in an observational sense, referring to a zone of reduced earthquake occurrence within the available catalog, without implying the absence of a slab or future rupture potential by default.

It is important to separate the observational "seismic gap' described here from the idea of a slab hole or slab gap, because the two terms refer to fundamentally different geodynamic scenarios. A seismic gap can represent a strongly coupled or "welded" segment of the plate interface where elastic strain accumulates and may be released in a future rupture (**Kanamori, 1981; Ritsema et al., 2012; Scholz, 2002**). By contrast, a slab hole implies a physical break or tearing within the subducting plate, potentially linked to thermal weakening, slab rollback, or changes in mantle flow, and is commonly associated with persistently reduced seismicity over longer timescales (**Miller et al., 2006; Rosenbaum et al., 2008; Widiyantoro et al., 2011**).

Recent seismic tomography studies beneath southern and central Java have proposed along-strike slab segmentation and possible tearing at depths broadly comparable to the seismicity reduction observed here (**Widiyantoro et al., 2020, 2022, 2024**). While the present seismicity patterns are compatible with these models, they do not independently confirm slab tearing. Alternative explanations—including aseismic slip, elevated pore-fluid pressures, thermal weakening, or stress shadow effects following large earthquakes—may also produce reduced seismicity at intermediate depths without requiring slab (**Ji et al., 2017; Saffer & Tobin, 2011; Wang et al., 2003**).

The confinement of reduced seismicity to the central Java (B–B′) segment, and its absence in the western (A–

A′) and eastern (C–C′) profiles, indicates pronounced along-strike heterogeneity in slab geometry, hydration state, or mechanical coupling along the Sunda margin. Such heterogeneity is well documented in the subduction systems worldwide and has also been emphasized for Java, where along-strike differences in incoming-plate age, sediment thickness, and inherited oceanic fabric can strongly modulate slab behaviour (**Muttaqy et al., 2023; Penniston-Dorland et al., 2015; Supendi et al., 2023**).

From the stress-field perspective, event-based orientations inferred from focal mechanisms do not show an abrupt or systematic rotation that coincides with the seismic-gap area. This suggests that the reduced intermediate-depth seismicity is unlikely to mark a major boundary between stress regimes; instead, it may reflect more localized controls such as rheological contrasts of fluid-related processes within the slab or the mantle wedge (**Heidbach et al., 2010, 2018; Michael, 1987; Sperner et al., 2002**). Similar mismatches between stress orientation and seismicity density have been reported in other subduction zones where aseismic deformation and/or transient fluid processes play a dominant role (**Ide et al., 2007; Obara & Kato, 2016**).

In terms of hazard implications, the central Java segment stands in contrast to neighboring parts of the Sunda-Java trench, including the Pangandaran and Banyuwangi regions, which have produced large historical earthquakes and tsunamigenic events (**Abercrombie et al., 2001; Bilek & Lay, 2018**). However, the current catalog alone cannot determine whether the reduced seismicity beneath central Java indicates a locked segment capable of a future large rupture, or a predominantly aseismic zone. This uncertainty underscores the need for integrated, long-term constraints such as higher-resolution seismic tomography, geodetic coupling models, and fluid seismic imaging to better evaluate the seismic potential of this segment.

5.2. *Crustal Architecture Inferred from Integrated Gravity Analysis*

The gravity-anomaly patterns obtained in this study capture the same first-order features previously described for Java, including relatively high anomalies along the southern offshore margin and lower values beneath central Java (**Green et al., 1981; Guntoro, 1995; Handayani et al., 2022**). This agreement suggests that the satellite-based dataset and our processing workflow produce results that are consistent with established regional gravity models. Additional cross-checking against Complete Bouguer Aomaly (CBA) maps published by the Geological Survey of Indonesia (PSG) supports the robustness of the large-scale anomaly pattern, particularly the contrast among the southern forearc, the central Java Basin, and the northern Java domain (**Handayani et al., 2022; PSG, 2018**).

We applied RAPS-based spectral decomposition to separate the gravity field into regional (long-wavelength, deep) and residual (short-wavelength, shallow) components (**Banerjee & SubbaRao, 2020; Spector & Grant, 1970**). This approach offers a consistent basis for integrating gravity with seismicity and stress data across the full study area and helps avoid biases caused by non-uniform filtering or gridding practices used in some previous studies.

Regional anomalies emphasize large-scale along-arc changes in crustal thickness and lithospheric density, while residual anomalies bring out localized density variations associated with volcanic centers, forearc features, and the Java Back-Arc Thrust. Gravity results alone do not diagnose slab tearing or slab continuity, but they constrain crustal architecture in a way that can be tested against seismic observations. The transition from moderate to low residual anomalies beneath central Java to higher values to the west and east coincides with along-strike seismicity variability, including the seismic gap along B-B'. This pattern is more consistent with lateral changes in crustal thickness, sedimentary basin development, or lithospheric density that may affect coupling or stress transfer, rather than directly indicating slab sementation (**Supendi et al., 2023; Widiyantoro et al., 2020**).

Residual gravity highs of 50 mGal along the southern margin align with the subduction front and accretionary prism, where relatively dense oceanic lithosphere is underthrust beneath the Sunda margin. In contrast, strong residual lows (down to -44 mGal) beneath central Java delineate the Java Basin, consistent with thick accumulations of low-density sedimentary fill. A frontal residual high of 31 mGal further marks the compressional forearc prism, in line with active shortening and ongoing accretion along the margin. Overall, these patterns agree with gravity-based interpretations from regional and global satellite models, including EGM2008-2020, GRACE, and TOPEX/GEOSAT-derived products, which are widely used to image subduction-related density contrasts in tectonically complex settings worldwide (**Förste et al., 2014; Hirt et al., 2011; Sandwell et al., 2014; Wu et al., 2021**).

A pronounced outer gravity high south of the trench is interpreted to reflect lithospheric flexure and plate bending before subduction, reproducing the classic arc-trench gravity couple observed at many convergent margins. Comparable patterns have been documented in recent gravity studies from Indonesia and other subduction systems, where outer rise gravity highs are commonly linked to elastic bending and density redistribution within the downgoing plate (**Capitanio et al., 2025; Oliveira et al., 2015; Zuhair et al., 2022**).

Overall, the crustal architecture inferred from gravity provides important context but does not, on its own, diagnose slab segmentation. When considered together with seismicity, stress orientations, and seismic reflection interpretations, the gravity results help clarify why deformation style and seismic behaviour change along

Table 1: Comparison of Moho depth results using the RAPS method with CRUST 1.0 and the receiver function method.

Area	Longitude	Latitude	RAPS (Moho Depth, km)	Crust 1.0 (Moho Depth, km)	Receiver Function (Moho Depth, km)	Source
BLSI (Sumatera -Lampung)	105.15	-5.36	30	27	32	(**Bahri et al., 2021**)
SBJI (Jakarta)	106.06	-6.09	30	26	30 46	(**Syuhada & Anggono, 2016**) (**Bahri et al., 2021**)
CNJI (West Java)	107.54	-7.39	33.57	22.13	32 38	(**Syuhada & Anggono, 2016**) (**Bahri et al., 2021**)
CMJI (West Java)	107.54	-7.39	33.58	21.24	34.5 38	(**Syuhada & Anggono, 2016**) (**Bahri et al., 2021**)
SMRI (Central Java)	110.29	-7.08	38.35	21.24	36 37	(**Bahri et al., 2021**) (**Amukti et al., 2019**)
SIJM (East Java)	110.29	-7.077	38.35	21.24	30 40	(**Bahri et al., 2021**) (**Susena et al., 2023**)
SRBI (Bali)	115.17	-8.10	37.03	21.24	35	(**Bahri et al., 2021**)

strike beneath Java. This integrated view underscores how variations in crustal thickness, basin development, and lithospheric flexure can modulate stress transmission and the spatial expression of seismicity along the Sunda margin, with direct relevance to regional earthquake and tsunami hazard assessments.

5.3. *Moho Topography and Its Tectonic Significance*

The RAPS-derived Moho map (see **Figure 11**) gives a first-order view of how crustal thickness varies beneath Java and nearby margins. For most areas, the Moho is estimated at roughly 30-40 km depth (see **Table 1**), which aligns well with independent constraints from receiver functions, global crustal compilation, and regional seismic studies (**Amukti et al., 2019; Bahri et al., 2021; Laske et al., 2013; Susena et al., 2023; Syuhada & Anggono, 2016**). This level of agreement suggests that the gravity-based spectral estimates are robust at the scale of the present analysis.

5.3.1. RAPS Parameters and Methodological Considerations

We performed RAPS using sliding spectral windows of 150-250 km, following the established approach for Moho estimation in tectonically complex regions (**Banerjee & SubbaRao, 2020; Spector & Grant, 1970**). Long-wavelength CBA components were extracted using low-wavenumber cutoffs to target deep density contrasts at the crust-mantle boundary. We assumed a density contrast of 0.3-0.4 g/cm^3 between the lower crust and upper mantle, consistent with common practice in gravity-based Moho studies (**Bassett & Watts, 2015; Hinze, 2003**). These parameter choices limit resolution but remain suitable for first-order lithospheric-scale Moho mapping.

5.3.2. Moho Shallowing Near the Trench: Interpretation and Limitations

The apparent Moho shallowing to 11-15 km in the vicinity of the Sunda-Java trench should be interpreted with caution. Such values should not be viewed as precise Moho depths but rather as effective crustal thickness estimates influenced by strong lateral density contrasts, slab-related mass anomalies, and spectral leakage effects near the subduction front. Similar apparent Moho shallowing has been reported in other subduction margins where gravity spectra are affected by the juxtaposition of oceanic lithosphere, accretionary prisms, and forearc basins (**Bassett & Watts, 2015; Van Rijsingen et al., 2018**). The shallow RAPS-derived depths likely reflect the transition from continental crust beneath Java to oceanic lithosphere at the trench, rather than an anomalously thin crust alone.

5.3.3. Cross-Validation with Seismic Reflection and Earthquake Data

Direct comparison with seismic reflection profiles (e.g. D-D', E–E′, F–F′, and G-G') shows that the gravity-derived Moho surface broadly coincides with the deepest laterally coherent reflector terminations and changes in seismic character at large two-way travel times. Although seismic profiles are reported in the time domain, the spatial correspondence between deep reflector truncations and gravity-inferred Moho variations supports the integrated interpretation. Furthermore, the distribution of intermediate- to deep-focus earthquakes defining the Wadati–Benioff zone provides an independent constraint on slab geometry beneath central and southern Java (**Supendi et al., 2023; Widiyantoro et al., 2020**).

5.3.4. Tectonic Implications and Along-Strike Variability

The lateral variation in Moho depth along Java mirrors the along-strike heterogeneity observed in seismic-

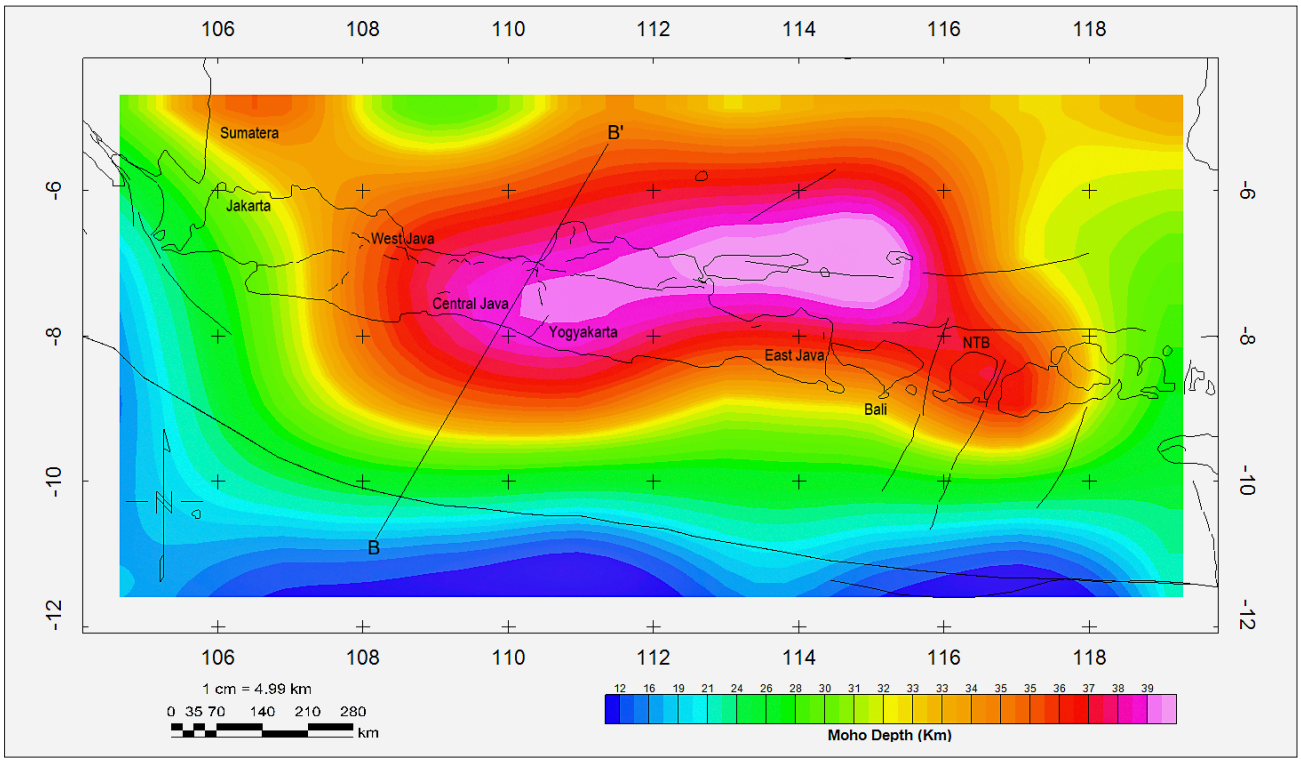


Figure 11: Moho depth distribution across the Southern Sunda Arc derived from Radially Averaged Power Spectrum (RAPS) analysis of the Complete Bouguer Anomaly. The black line B–B′ marks the transect used to extract the Moho-depth profile shown in **Figure 12**. Moho depth values are reported in kilometers (km).

ity patterns and gravity anomalies. Thicker crust beneath central and southern Java corresponds to regions of reduced intermediate-depth seismicity (Section B–B′), while comparatively thinner crust toward the trench and northern Java coincides with higher gravity anomalies and different deformation styles. This spatial association implies a mechanical connection among crustal segmentation, slab geometry, and the regional stress field, consistent with recent geodynamic models that emphasize slab bending, segmentation, and along-strike variations in coupling along the Sunda margin (**Lallemand et al., 2018; Supendi et al., 2023; Widiyantoro et al., 2024**).

5.4. *Seismic Reflection Profiles in a Regional Framework and Integrated Tectonic Synthesis*

The seismic reflection profiles examined in this image show structural architectures that align well with established interpretations of the Sunda-Java subduction system, including accretionary prisms, forearc basin, uplifted outer highs, deformation within the volcanic arc, and back-arc thrusting (**Kopp et al., 2006; Patria & Aulia Nur, 2020; Singh et al., 2011; Susilohadi, 2020**). These features have been widely reported across both erosional and accretionary segments of the Java margin and therefore provide a solid basis for regional-scale tectonic interpretation.

5.4.1. Southern Java: Accretionary Prism and Forearc Architecture (D–D′)

The D-D' seismic line (see **Figure 9**) images a clear accretionary prism at the frontal margin, followed landward by a forearc basin situated roughly 50-140 km from the trench. Reflections within the basin are concentrated at 3000-5000 ms two-way travel time (TWT), consistent with a thick sedimentary package overlying the subduction interface. Seaward, the basin is confined by an uplifted outer forearc high, toward which landward-dipping strata locally onlap. This reflector geometry points to forearc doming and uplift features commonly associated with erosional margins, where strong plate coupling and basal erosion play an important role (**Bassett & Watts, 2015; Kopp et al., 2006; Lallemand et al., 2018**). Comparable forearc configurations have been described offshore central and southern Java, supporting the view that the D-D' profile records long-lived, subduction-driven deformation rather than a localized anomaly.

5.4.2. Central Java: Back-Arc Thrusting and Upper-Plate Shortening (F–F′)

The F-F' (see **Figure 10**) near Mount Slamet shows a major thrust system, reflecting strong upper-plate compression. The thrust defines a clear boundary between volcanic and sedimentary units and is interpreted as part of the Java Back-Arc Thrust. The volcanic edifice occupies the hanging wall and overrides sedimentary layers,

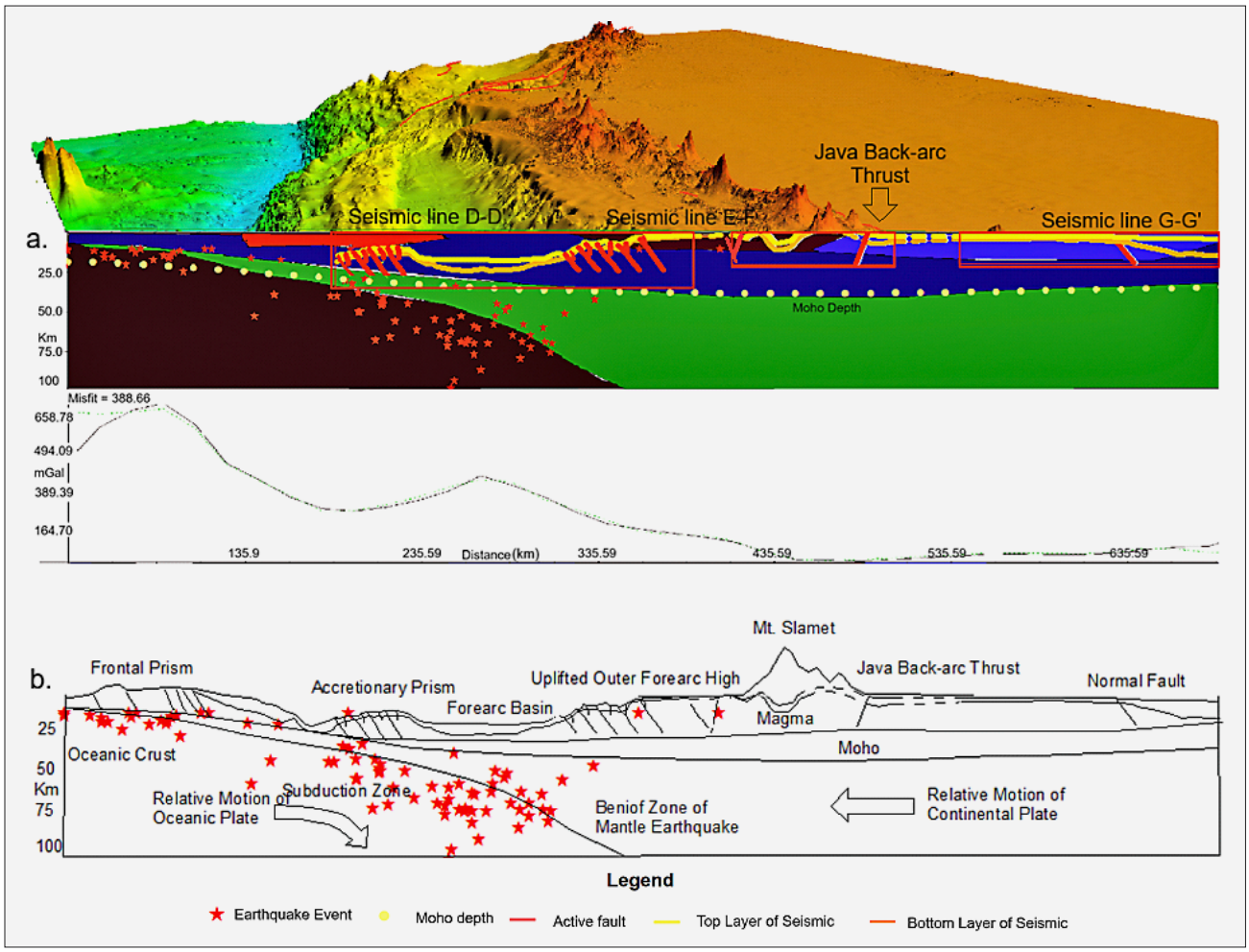


Figure 12: Geophysical integration along B-B'. (a) Overlaid datasets: topography, gravity anomalies, earthquake hypocenters (red stars), interpreted horizons from PSTM reflection profiles (upper: yellow; lower: orange), active faults (red lines), and Moho depths from RAPS (yellow circles). (b) Resulting tectonic synthesis for the Southern Sunda Arc derived from the integrated dataset.

a configuration consistent with arc-parallel shortening related to ongoing Indo-Austarlian-Eurasian convergence (**Aribowo et al., 2022; Widiyantoro et al., 2020**). Shallow folds at 1000-2000 ms TWT also indicate active shortening in the upper crust. Back-arc thrusting is widely recognised as a key inboard strain-accommodation mechanism in Java and other convergent margins (**Hall & Smyth, 2008; Lallemand et al., 2018; Supendi et al., 2023**).

5.4.3. Northern Java: Sedimentary Basins and Extensional Structures (G–G′)

The G-G' profile, which runs from Mount Muria northward toward the Java Sea, images a thick and laterally extensive sedimentary succession dominated by subhorizontal to gently dipping reflectors. This reflection style agrees with earlier interpretations that place northern Java in a transitional setting between the volcanic arc and the back-arc basins (**Kopp et al., 2006; Susilohadi, 2020**). Fault-related breaks seen as reflector offsets and localized loss of continuity are mainly extensional and are interpreted as normal faults. These structures likely record flexural and gravitational adjustments within the upper plate, superimposed on the broader compressional regime that characterizes the Sunda margin (**Patria & Aulia Nur, 2020; Singh et al., 2011**).

5.5. *Integrated Tectonic Synthesis and Conceptual Model*

By integrating earthquake distributions, focal-mechanism-based stress orientations, gravity anomalies, RAPS-derived Moho depth estimates, and 2D seismic reflection profiles (see **Figure 12**), this study develops a coherent regional tectonic synthesis for southern and central Java. Taken together, the results support an along-strike heterogeneous subduction model, in which slab geometry, mechanical coupling, crustal thickness, and upper-plate deformation vary systematically along the Sunda-Java margin.

Rather than proposing entirely new tectonic components, this work refines existing concepts by explicitly

connecting multiple independent geophysical observations within a consistent spatial framework. The integrated comparison helps clarify how reduced- seismicity zones, lateral Moho undulations, gravity domains, stress orientations, and mapped fault systems relate to one another, while also acknowledging key limitations related to data resolution, catalog length, and the inherent non-uniqueness of potential-field interpretation (**Heidbach et al., 2010; Lallemand et al., 2018; Widiyantoro et al., 2020**).

5.5.1. Integrated Tectonic Architecture of Southern Java

The integrated tectonic model (see **Figure 12**) brings together seismicity patterns, gravity-inferred crustal architecture, seism-reflection geometry, topography, and Moho-depth estimates into a single conceptual framework. It portrays an active subduction system in which the Indo-Australian Plate descends beneath the Eurasian margin, producing recurrent seismicity and the development of a frontal prism and forearc basins. Offshore southern Java, the E-E' profile images a characteristic trench-toe accretionary prism and a forearc basin positioned 50-140 km landward of the trench, with strong reflectors at 300-500 ms TWT and an uplifted outer forearc high. This configuration is consistent with eorional-margin behaviour reported for central and eastern Java (**Bassett & Watts, 2015; Kopp et al., 2006; Patria & Aulia Nur, 2020**).

Farther landward, the forearc (Java) basin is associated with gravity lows and thick sedimentary packages. In contrast, gravity highs and folding beneath Mount Slamet suggest a volcanic plateau and localized crustal thickening. North of Slamet, seismic line F-G outlines the Java Back-Arc Thrust system, reflecting arc-parallel shortening and inboard thrusting that accommodates convergence-related strain within the upper plate (**Aribowo et al., 2022; Hall & Smyth, 2008; Supendi et al., 2023**). The modelled Moho surface shows progressive shoaling toward the trench and thickening to 35-40 km beneath Java, consistent with receiver-function constraints and global crustal models (**Bahri et al., 2021; Laske et al., 2013; Syuhada & Anggono, 2016**).

5.5.2. Integration with Seismicity and Stress-Field Observations

The distribution of shallow to intermediate-depth earthquakes, together with stress orientations inferred from focal mechanisms, is broadly kinematically consistent with the structural framework indicated by the gravity and seismic- reflection interpretations. The coexistence of trench-parallel and trench-normal stress components reflects the combined effects of plate convergence, slab bending, and upper-plate deformation. Notably, the lack of an abrupt stress-regime change across the reduced-seismicity corridor suggests that the observed seismic gap does not necessarily mark a major mechanical discontinuity (**Heidbach et al., 2010; Michael, 1987; Sperner et al., 2002**).

Residual gravity anomalies also show clear spatial correspondence with the principal tectonic domains imaged on the seismic profiles, including forearc highs, sedimentary basins, volcanic centers, and back-arc thrust zones (**Handayani et al., 2022; PSG, 2018**). Although gravity data alone cannot uniquely resolve slab tearing or mechanical decoupling, integrating them with seismicity patterns and structural observations provides valuable constraints on crustal architecture and potential lithospheric segmentation (**Banerjee & SubbaRao, 2020; Spector & Grant, 1970**).

5.6. Active Fault Systems: From Trench to Back-Arc

Java's tectonic framework is governed by the oblique subduction of the Indo-Australian Plate beneath the Eurasian (Sunda) Plate, which generates a spectrum of active fault systems extending from the Sunda-Java Trench to the back-arc domain. Along the trench, convergence rates of 60-70 mm/yr (**Koulali et al., 2016**) promote thrust faulting and the growth of accretionary prisms characterized by imbricate structures and locally developed strike-slip components (**Kopp et al., 2006**). These frontal fault systems host major megathrust earthquakes, including the 1994 Banyuwangi and 2006 Pangandaran events, where slip occurred along shallow-dipping (< 15 °) plate interfaces. Landward of the trench, the forearc prism and outer arc highs are expressed by compressional ridges and frontal gravity highs of 30-50 mGal, reflecting ongoing crustal shortening and sediment accretion (**Guntoro, 1995; Simandjuntak, 1993**). In contrast, the Java Basin is marked by pronounced residual gravity lows (-40 mgal) associated with thick sedimentary successions, while seismic reflection data reveal reverse and fold-related faulting within the basin fill (**Patria & Aulia Nur, 2020**). Together, these observations indicated that the frontal and forearc regions constitute the primary zones of strain accumulation driven by plate coupling, sediment accretion, and basal shear along the Sunda margin (**Hall et al., 2011; Hamilton, 1970; Kopp et al., 2006**).

Farther inland, within the inner arc and back-arc regions, deformation styles evolve from dominantly compressional to transpressional and locally extensional regimes, reflecting spatial variations in plate coupling and rollback dynamics. The Cilacap-Slamet Zone and the Semarang-Kendal fault system display oblique thrusting and strike-slip motion that accommodate trench-parallel shear (**Hall et al., 2011; Patria & Aulia Nur, 2020**). Seismic and gravity evidence identify the Java Back-Arc (JBT) as the principal compressional structure separating the volcanic arc from the northern back-arc basin (**Aribowo et al., 2022; Guntoro, 1995; Smyth et al., 2008**). Further north, normal faults and strike-slip faults

dominate the Java Basin, reflecting extensional reactivation and differential crustal loading following subduction (**Kopp et al., 2006**). Integration of focal mechanism solutions, Moho topography, and gravity anomalies confirms a progressive transition from compression perpendicular to the trench to shear and extensional deformation on land, consistent with regional models of arc segmentation and forearc evolution (**Hamilton, 1970; Simandjuntak, 1993**). This pattern of trench-to-backarc deformation underscores the complex interactions between subduction dynamics, crustal rheology, and plate reconfiguration, with direct implications for seismic and tsunami hazards across the South Sunda Arc.

5.7. Limitations, Implications, and Future Directions

The lack of time-to-depth conversion and direct well ties prevents quantitative estimates of fault depth and displacement; accordingly, our interpretations are limited to time-domain geometry and regional-scale synthesis. Data quality beneath the volcanic region is uneven, and structural interpretations in these areas are inherently non-unique. Even so, the combined dataset provides a solid tectonic framework in which seismic reflection profiles act as a key link between surface deformation, gravity-inferred crustal architecture, Moho geometry, and subduction-related geodynamics.

Taken together, the RAPS-derived Moho relief, gravity anomaly patterns, seismic reflection geometries, stress orientations, and earthquake distributions support a coherent framework in which subduction-driven crustal deformation varies systematically along strike. While gravity-based Moho estimates alone cannot determine whether slab tearing occurs or explain the origin of the seismic gap, integrating these results with seismicity and structural observations offers important constraints on lithospheric segmentation and tectonic evolution along the Sunda-Java margin. Future work that combines higher-resolution seismic tomography, denser receiver-function coverage, and geodetic observations will be essential to refine these interpretations and to test the proposed links among Moho geometry, slab dynamics, and seismic hazard.

6. Conclusions

Our study integrates seismicity analysis (2000-2023), gravity anomalies, RAPS-based Moho depth estimates, and 2D seismic reflection interpretation to better constrain the tectonic architecture of Java Island and the Southern Sunda Arc. The earthquake catalog highlights a marked reduction in intermediate-depth seismicity beneath southern Java (a seismic gap), which may reflect along-strike heterogeneity in slab behaviour such as localized weakening/segmentation or dominantly aseismic deformation within the subducting Indo-Australian Plate. Gravity anomalies delineate the main tectonic domains, with higher values associated with the offshore subduction-front region and lower anomalies outlining the sediment-filled Java Basin. Seismic reflection interpretation further resolves key structural elements, including a frontal prism, fold-related deformation, the onshore Java Back-Arc Thrust, and normal faulting in the northern offshore sector. The profiles image a classic trench-to-forearc architecture, with an accretionary prism at the trench toe, a forearc basin located 50-140 km landward, uplifted outer forearc highs, and a back-arc thrust zone north of Mount Slamet. Moho depth estimates from the RAPS method indicate crustal thicknesses of roughly 30-40 km beneath most of Java. Collectively, these observations emphasize strong along-strike variability in subduction-related deformation and clarify the links between forearc evolution and back-arc shortening, providing an improved geophysical framework for evaluating earthquake and tsunami potential in southern Indonesia.

Acknowledgement

We sincerely appreciate the insightful feedback and valuable suggestions from the reviewers, which have significantly contributed to the refinement of this research. We extend our gratitude to King Abdulaziz University for supporting this study by providing a license for the Petrel software used in the analysis. We also acknowledge the Indonesian National Research and Innovation Agency (BRIN) for supplying gravity software licenses, as well as Pusdatin, Ministry of Energy and Mineral Resources of the Republic of Indonesia, for their support in providing two-dimensional seismic data essential to this research.

7. References

Abercrombie, R. E., Antolik, M., Felzer, K., & Ekström, G. (2001). The 1994 Java tsunami earthquake: Slip over a subducting seamount. *Journal of Geophysical Research*, *106*, 6595–6607.

Amukti, R., Yunartha, N. A., Anggraini, A., & Suryanto, W. (2019). Modeling of the earth's crust and upper mantle beneath central part of Java Island using receiver function data. *AIP Conference Proceedings*, *2194*. https://doi.org/10.1063/1.5139736

Aribowo, S., Husson, L., Natawidjaja, D. H., Authemayou, C., Daryono, M. R., Puji, A. R., Valla, P. G., Pamumpuni, A., Wardhana, D. D., de Gelder, G., Djarwadi, D., & Lorcery, M. (2022). Active Back-Arc Thrust in North West Java, Indonesia. *Tectonics*, *41*(7). https://doi.org/10.1029/2021TC007120

Bahri, S., Suryanto, W., & Ngadmanto, D. (2021). *Sediment Thickness and Moho Depth Beneath Western Indonesian Region From Teleseismic Receiver Function*. https://doi.org/10.21203/rs.3.rs-356661/v1

Banerjee, A., & SubbaRao, P. B. V. (2020). Depth estimation of subsurface discontinuity by applying spectral analysis of gravity data in sub-basalt region of Kutch-Saurashtra. *Geohorizon*, 26–30.

Bassett, D., & Watts, A. B. (2015). Gravity anomalies, crustal structure, and seismicity at subduction zones: 1. Seafloor roughness and subducting relief. *Geochemistry, Geophysics, Geosystems*, *16*(5), 1508–1540. https://doi.org/10.1002/2014GC005684

Bilek, S. L., & Lay, T. (2018). Subduction zone megathrust earthquakes. *Geosphere*, *14*(4), 1468–1500. https://doi.org/10.1130/GES01608.1

Capitanio, F. A., Gollapalli, T., M, R., Graciosa, J. C., Mohd, Z., Beall, A., & Dal Zilio, L. (2025). Bridging the gap between subduction dynamics and the long-term strength of the Sunda megathrust. *Nature Communications*, *16*(1), 10781. https://doi.org/10.1038/s41467-025-65824-7

Dziewonski, A. M., Chou, T. A., & Woodhouse, J. H. (1981). Determination of earthquake source parameters from waveform data for studies of global and regional seismicity. *Journal of Geophysical Research*, *86*(B4), 2825–2852. https://doi.org/10.1029/JB086iB04p02825

Ekström, G., Nettles, M., & Dziewoński, A. M. (2012). The global CMT project 2004-2010: Centroid-moment tensors for 13,017 earthquakes. *Physics of the Earth and Planetary Interiors*, *200–201*, 1–9. https://doi.org/10.1016/j.pepi.2012.04.002

Eshagh, M., Hussain, M., Tenzer, R., & Romeshkani, M. (2016). Moho density contrast in central Eurasia from GOCE gravity gradients. *Remote Sensing*, *8*(5). https://doi.org/10.3390/rs8050418

Exploration Unit EP III. (1990). *Final Report of Exploration Well*.

Förste, C., Bruinsma, S., Abrikosov, O., Flechtner, F., Marty, J.-C., Lemoine, J.-M., Dahle, C., Neumayer, H., Barthelmes, F., König, R., & Biancale, R. (2014). EIGEN-6C4-The latest combined global gravity field model including GOCE data up to degree and order 1949 of GFZ Potsdam and GRGS Toulouse. In *Geophysical Research Abstracts* (Vol. 16). http://icgem.gfz-potsdam.de

Green, R., Adkins, J. S., Harrington, H. J., & Untung, M. (1981). Bouguer gravity map of Indonesia. *Tectonophysics*, *71*, 267–280.

Guntoro, A. (1995). *Tectonic Evolution And Crustal Structure Of The Central Indonesian Region From Geology, Gravity And Other Geophysical Data* [Thesis]. University of London.

Hall, R., Cottam, M. A., & Wilson, M. E. J. (2011). The SE Asian gateway: History and tectonics of the Australia-Asia collision. *Geological Society Special Publication*, *355*, 1–6. https://doi.org/10.1144/SP355.1

Hall, R., & Smyth, H. R. (2008). Cenozoic arc processes in Indonesia: Identification of the key influences on the stratigraphic record in active volcanic arcs. *Special Paper of the Geological Society of America*, *436*, 27–54. https://doi.org/10.1130/2008.2436(03)

Hamilton, W. (1970). Tectonic Map of Indonesia. *U.S Geological Survey*.

Handayani, L., Hanif, M., Arisbaya, I., & Gaol, K. L. (2022). Comparative study of edge enhancement techniques of the Java arc gravity anomalies. *AIP Conference Proceedings*, *2652*. https://doi.org/10.1063/5.0106232

Hanif, M., Handayani, L., Rizkita Puji, A., Patria, A., & Ramdhan, M. (2024). Gravity Modelling Insights into Crustal Structure: Moho Depth and Subsurface Structures in Central Sulawesi. *IOP Conference Series: Earth and Environmental Science*, *1373*(1). https://doi.org/10.1088/1755-1315/1373/1/012050

Harding, T. P., & Lowell, J. D. (1979). *Structural Styles, Their Plate-Tectonic Habitats, and Hydrocarbon Traps In Petroleum Provinces^* (Issue 7). http://pubs.geoscienceworld.org/aapg/aapgbull/article-pdf/63/7/1016/4448497/aapg_1979_0063_0007_1016.pdf

Hayes, G. P., Moore, G. L., Portner, D. E., Hearne, M., Flamme, H., Furtney, M., & Smoczyk, G. M. (2018). Slab2, a comprehensive subduction zone geometry model. *Science*, *362*(6410), 58–61. https://doi.org/10.1126/science.aat4723

Heidbach, O., Rajabi, M., Cui, X., Fuchs, K., Müller, B., Reinecker, J., Reiter, K., Tingay, M., Wenzel, F., Xie, F., Ziegler, M. O., Zoback, M. Lou, & Zoback, M. (2018). The World Stress Map database release 2016: Crustal stress pattern across scales. In *Tectonophysics* (Vol. 744, pp. 484–498). Elsevier B.V. https://doi.org/10.1016/j.tecto.2018.07.007

Heidbach, O., Tingay, M., & Wenzel, F. (2010). Frontiers in Stress Research. In *Tectonophysics* (Vol. 482, Issues 1–4, pp. 1–2). https://doi.org/10.1016/j.tecto.2009.11.009

Helmholtz-Zentrum Potsdam. (2024). *GEOFON Program GFZ Potsdam __ Earthquake Information Service*. Postdam.

Herninda, G., & Mohamad, F. (2021). Petrofisika Reservoir Sand A Formasi Talang Akar Berdasarkan Data Well Log Di Lapangan "Fr", Cekungan Asri. *Padjadjaran Geoscience Journal*, *5*(1), 24–33.

Hinze, W. J. (2003). Bouguer reduction density, why 2.67? *Geophysics*, *68*(5), 1559–1560. https://doi.org/10.1190/1.1620629

Hirt, C., Gruber, T., & Featherstone, W. E. (2011). Evaluation of the first GOCE static gravity field models using terrestrial gravity, vertical deflections and EGM2008 quasigeoid heights. *Journal of Geodesy*, *85*(10), 723–740. https://doi.org/10.1007/s00190-011-0482-y

Houston, H. (2007). *4.11 Deep Earthquakes* (pp. 339–340). Elsevier.

Hutchings, S. J., & Mooney, W. D. (2021). The Seismicity of Indonesia and Tectonic Implications. *Geochemistry, Geophysics, Geosystems*, *22*(9). https://doi.org/10.1029/2021GC009812

Ide, S., Beroza, G. C., Shelly, D. R., & Uchide, T. (2007). A scaling law for slow earthquakes. *Nature*, *447*(7140), 76–79. https://doi.org/10.1038/nature05780

Isacks, B. (1971). *Distribution of Stresses in the Descending Lithosphere from a Global Survey of Focal-Mechanism Solutions of Mantle Earthquakes* (Vol. 9, Issue 1).

Jambak, M. A., Syafri, I., Isnaniawardhani, V., Benyamin, & Rodriguez, H. (2015). Facies and diagenetic level of the

Upper Cibulakan and Parigi Formation, in Randegan and Palimanan Area. *Indonesian Journal on Geoscience*, *2*(3), 157–166. https://doi.org/10.17014/ijog.2.3.157-166

Ji, Y., Yoshioka, S., & Banay, Y. A. (2017). Thermal State, Slab Metamorphism, and Interface Seismicity in the Cascadia Subduction Zone Based On 3-D Modeling. *Geophysical Research Letters*, *44*(18), 9242–9252. https://doi.org/10.1002/2017GL074826

Kanamori, H. (1981). The Nature Of Seismicity Patterns Before Large Earthquakes. In *Earthquake Prediction: An International Review. American Geophysical Union* (Vol. 4, pp. 1–19).

Karner, G. D., & Watts, A. B. (1983). Gravity Anomalies and Flexure of the Lithosphere at Mountain Ranges. In *Journal of Geophysical Research* (Vol. 88, Issue B12).

Kopp, H., Flueh, E. R., Petersen, C. J., Weinrebe, W., Wittwer, A., & Scientists, M. (2006). The Java margin revisited: Evidence for subduction erosion off Java. *Earth and Planetary Science Letters*, *242*(1–2), 130–142. https://doi.org/10.1016/j.epsl.2005.11.036

Koulali, A., Susilo, S., McClusky, S., Meilano, I., Cummins, P., Tregoning, P., Lister, G., Efendi, J., & Syafi'I, M. A. (2016). Crustal strain partitioning and the associated earthquake hazard in the eastern Sunda-Banda Arc. *Geophysical Research Letters*, *43*(5), 1943–1949. https://doi.org/10.1002/2016GL067941

Lallemand, S., Peyret, M., van Rijsingen, E., Arcay, D., & Heuret, A. (2018). *Roughness Characteristics of Oceanic Seafloor Prior to Subduction in Relation to the Seismogenic Potential of Subduction Zones*. *19*(7), 2121–2146. https://doi.org/10.1029/2018GC007434ï

Laske, G., Masters, G., Ma, Z., & Pasyanos, M. (2013). Update on Crust 1.0-A 1-degree Global Model of Earth's Crust. *Geophys, Rest*.

Lemenkova, P. (2020). Java and sumatra segments of the sunda trench: Geomorphology and geophysical settings analysed and visualized by GMT. *Bulletin of the Serbian Geographical Society*, *100*(2), 1–23. https://doi.org/10.2298/GSGD2002001L

Michael, A. J. (1987). Use of Focal Mechanisms to Determine Stress: A Control Study. In *Journal of Geophysical Research* (Vol. 92, Issue B1).

Miller, M. S., Gorbatov, A., & Kennett, B. L. N. (2006). Three-dimensional visualization of a near-vertical slab tear beneath the southern Mariana arc. *Geochemistry, Geophysics, Geosystems*, *7*(6). https://doi.org/10.1029/2005GC001110

Muttaqy, F., Nugraha, A. D., Puspito, N. T., Sahara, D. P., Zulfakriza, Z., Rohadi, S., & Supendi, P. (2023). Double-difference earthquake relocation using waveform cross-correlation in Central and East Java, Indonesia. *Geoscience Letters*, *10*(1). https://doi.org/10.1186/s40562-022-00259-2

Obara, K., & Kato, A. (2016). Connecting slow earthquakes to huge earthquakes. In *Science (New York, N.Y.)* (Vol. 353, Issue 6296, pp. 253–257). https://doi.org/10.1126/science.aaf1512

Oliveira, P. H. S., Ferreira, J. M., Bezerra, F. H. R., Assumpção, M., Do Nascimento, A. F., Sousa, M. O. L., & Menezes, E. A. S. (2015). Influence of the continental margin on the stress field and seismicity in the intraplate Acaraú Seismic Zone, NE Brazil. *Geophysical Journal International*, *202*(3), 1453–1462. https://doi.org/10.1093/gji/ggv211

Patria, A., & Aulia Nur, A. (2020). Structural And Earthquake Evaluations Along Java Subduction Zone, Indonesia. *RISET Geologi Dan Pertambangan*, *30*(1), 65–79. https://doi.org/10.14203/risetgeotam2020.v30.1074

Penniston-Dorland, S. C., Kohn, M. J., & Manning, C. E. (2015). The global range of subduction zone thermal structures from exhumed blueschists and eclogites: Rocks are hotter than models. *Earth and Planetary Science Letters*, *428*, 243–254. https://doi.org/10.1016/j.epsl.2015.07.031

PSG, P. S. G. (2018). *Complete Bouguer Anomaly Map of Indonesia*.

Ritsema, J., Lay, T., & Kanamori, H. (2012). The 2011 Tohoku earthquake. In *Elements* (Vol. 8, Issue 3, pp. 183–188). Mineralogical Society of America. https://doi.org/10.2113/gselements.8.3.183

Rosenbaum, G., Gasparon, M., Lucente, F. P., Peccerillo, A., & Miller, M. S. (2008). Kinematics of slab tear faults during subduction segmentation and implications for Italian magmatism. *Tectonics*, *27*(2). https://doi.org/10.1029/2007TC002143

Roy, A., Prasad, K. N. D., Sharma, R. K., Vijayakumar, D., & Kumar, R. (2025). CNN-Trained Centroid Method for Estimating Depth to the Bottom of the Magnetic Sources (DBMS) and Its Application to the Southern Indian Shield. *Journal of Geophysical Research: Solid Earth*, *130*(9). https://doi.org/10.1029/2024JB030918

Roy, A., Prasad, M., Padma Rao, B., & Tomson, J. K. (2023). Estimation of Moho Depth Beneath Southern Indian Shield by Inverting Gravity Anomalies Constrained by Seismic Data. *Journal of Geophysical Research: Solid Earth*, *128*(3). https://doi.org/10.1029/2022JB025651

Saffer, D. M., & Tobin, H. J. (2011). Hydrogeology and mechanics of subduction zone forearcs: Fluid flow and pore pressure. *Annual Review of Earth and Planetary Sciences*, *39*, 157–186. https://doi.org/10.1146/annurev-earth-040610-133408

Sandwell, D. T., Müller, R. D., Smith, W. H. F., Garcia, E., & Francis, R. (2014). New global marine gravity model from CryoSat-2 and Jason-1 reveals buried tectonic structure. *Science*, *346*(6205), 65–67. https://doi.org/10.1126/science.1258213

Schlüter, H. U., Gaedicke, C., Roeser, H. A., Schreckenberger, B., Meyer, H., Reichert, C., Djajadihardja, Y., & Prexl, A. (2002). Tectonic features of the southern Sumatra-western Java forearc of Indonesia. *Tectonics*, *21*(5), 11-1-11–15. https://doi.org/10.1029/2001TC901048

Scholz, C. H. (2002). *The Mechanics of Earthquakes and Faulting* (Second Edition). Cambridge University Press.

Shamim, S., Khan, P. K., & Mohanty, S. P. (2019). Stress reconstruction and lithosphere dynamics along the Sumatra subduction margin. *Journal of Asian Earth Sciences*, *170*, 174–187. https://doi.org/10.1016/j.jseaes.2018.11.008

Sherif, R. E., & Geldart, L. P. (1995). *Exploration Seismology* (Second). Cambridge University Press.

Simandjuntak, T. O. (1993). Neogene tectonics and orogenesis of Indonesia. *Bulletin of the Geological Society of Malaysia*, *33*, 43–64. https://doi.org/10.7186/bgsm33199305

Simandjuntak, T. O., & Barber, A. J. (2016). Contrasting tectonic styles in the Neogene orogenic belts of Indonesia. *Tectonic Evolution of Southeast Asia, Geological Society Special Publication*, 185–201. http://sp.lyellcollection.org/

Singh, S. C., Hananto, N., Mukti, M., Permana, H., Djajadihardja, Y., & Harjono, H. (2011). Seismic images of the megathrust rupture during the 25th October 2010 Pagai earthquake, SW Sumatra: Frontal rupture and large tsunami. *Geophysical Research Letters*, *38*(16). https://doi.org/10.1029/2011GL048935

Smyth, H. R., Hall, R., & Nichols, G. J. (2008). Cenozoic volcanic arc history of East Java, Indonesia: The stratigraphic record of eruptions on an active continental margin. *Special Paper of the Geological Society of America*, *436*, 199–222. https://doi.org/10.1130/2008.2436(10)

Spector, A., & Grant, F. S. (1970). Statistical Model For Interpreting Aeromagnetic Data. *Geophysics*, *32*(2), 293–302.

Sperner, B., Müller, B., Heidbach, O., Delvaux, D., Reinecker, J., & Fuchs, K. (2002). Tectonic stress in the Earth's crust: advances in the World Stress Map project. *New Insights into Structural Interpretation and Modelling. Geological Society. London.*, *212*, 101–116. http://www.soest.

Supendi, P., Nugraha, A. D., Puspito, N. T., Widiyantoro, S., & Daryono, D. (2018). Identification of active faults in West Java, Indonesia, based on earthquake hypocenter determination, relocation, and focal mechanism analysis. *Geoscience Letters*, *5*(1). https://doi.org/10.1186/s40562-018-0130-y

Supendi, P., Widiyantoro, S., Rawlinson, N., Yatimantoro, T., Muhari, A., Hanifa, N. R., Gunawan, E., Shiddiqi, H. A., Imran, I., Anugrah, S. D., Daryono, D., Prayitno, B. S., Adi, S. P., Karnawati, D., Faizal, L., & Damanik, R. (2023). On the potential for megathrust earthquakes and tsunamis off the southern coast of West Java and southeast Sumatra, Indonesia. *Natural Hazards*, *116*(1), 1315–1328. https://doi.org/10.1007/s11069-022-05696-y

Suppe, J. (1983). Geometry and Kinematics of Fault-Bend Folding. *American Journal of Science*, *283*, 684–721.

Susena, P. K. O., Ariyanto, P., Pranata, B., Daryono, & Adi, S. P. (2023). Depth Estimation of Moho Discontinuity Layer at 5 BMKG Seismic Stations in East Java Using Receiver Function Method. *IOP Conference Series: Earth and Environmental Science*, *1288*(1). https://doi.org/10.1088/1755-1315/1288/1/012007

Susilohadi. (2020). *Madura Strait And Bali Sea Shallow Seismic Atlas* (L. Arifin, M. Hanafi, D. Kusnida, & R. Rahardiawan, Eds.; First Edition). Pusat Penelitian Dan Pengembangan Geologi Kelautan. www.mgi.esdm.go.id

Syuhada, & Anggono, T. (2016). Crustal structure in the southern part of West Java based on analysis of teleseismic receiver function. *AIP Conference Proceedings*, *1711*. https://doi.org/10.1063/1.4941642

Tselentis, G.-A., Drakopoulos, J., & Dimitriadis2, K. (1988). A Spectral Approach To Moho Depths Estimation From Gravity Measurements In Epirus (Nw Greece). In *J. Phys. Earth* (Vol. 36).

USGS. (2023, March 26). *Earthquake Catalog*. United States Geological Survey. https://earthquake.usgs.gov/earthquakes/map

Van Rijsingen, E., Lallemand, S., Peyret, M., Arcay, D., Heuret, A., Funiciello, F., & Corbi, F. (2018). How Subduction Interface Roughness Influences the Occurrence of Large Interplate Earthquakes. *Geophysics, Geosystems*, *19*(8), 2342–2370. https://doi.org/10.1029/2018GC007618ï

Wang, K., Wells, R., Mazzotti, S., Hyndman, R. D., & Sagiya, T. (2003). A revised dislocation model of interseismic deformation of the Cascadia subduction zone. *Journal of Geophysical Research: Solid Earth*, *108*(B1). https://doi.org/10.1029/2001jb001227

Widiyantoro, S., Gunawan, E., Muhari, A., Rawlinson, N., Mori, J., Hanifa, N. R., Susilo, S., Supendi, P., Shiddiqi, H. A., Nugraha, A. D., & Putra, H. E. (2020). Implications for megathrust earthquakes and tsunamis from seismic gaps south of Java Indonesia. *Scientific Reports*, *10*(1). https://doi.org/10.1038/s41598-020-72142-z

Widiyantoro, S., Pesicek, J. D., & Thurber, C. H. (2011). Subducting slab structure below the eastern Sunda arc inferred from non-linear seismic tomographic imaging. *Geological Society Special Publication*, *355*, 139–155. https://doi.org/10.1144/SP355.7

Widiyantoro, S., Supendi, P., Ardianto, A., Baskara, A. W., Bacon, C. A., Damanik, R., Rawlinson, N., Gunawan, E., Sahara, D. P., Zulfakriza, Z., Husni, Y. M., & Lesmana, A. (2022). Implications for fault locking south of Jakarta from an investigation of seismic activity along the Baribis fault, northwestern Java, Indonesia. *Scientific Reports*, *12*(1). https://doi.org/10.1038/s41598-022-13896-6

Widiyantoro, S., Supendi, P., Rawlinson, N., Daryono, M. R., & Rosalia, S. (2024). A note on the seismicity of Sumatra, western Sunda Arc, Indonesia, in relation to the potential for back-arc thrusting. *Scientific Reports*, *14*(1). https://doi.org/10.1038/s41598-024-64076-7

Wu, Y., He, X., Luo, Z., & Shi, H. (2021). An Assessment of Recently Released High-Degree Global Geopotential Models Based on Heterogeneous Geodetic and Ocean Data. *Frontiers in Earth Science*, *9*. https://doi.org/10.3389/feart.2021.749611

Xuan, S., & Jin, S. (2022). Moho depth and crustal density structure in the Tibetan Plateau from gravity data modelling. *Journal of Asian Earth Sciences*, *233*. https://doi.org/10.1016/j.jseaes.2022.105261

Yilmaz, Ö. (2001). *Seismic Data Analysis: Processing, Inversion, and Interpretation of Seismic Data* (S. M. Doherty, Ed.; Vol. 1). SEG.

Zoback, M. D. (2010). *Reservoir Geomechanics*. Cambridge University Press.

Zuhair, M., Gollapalli, T., Capitanio, F. A., Betts, P. G., & Graciosa, J. C. (2022). The Role of Slab Steps on Tectonic Loading Along Subduction Zones: Inferences on the Seismotectonics of the Sunda Convergent Margin. *Tectonics*, *41*(9). https://doi.org/10.1029/2022TC007242

SAŽETAK

Integrirani geofizički pokazatelji strukture kore i heterogenosti duž pružanja ispod otoka Java, južni dio Sundskoga luka

Južna i središnja Java smještene su duž subdukcijskoga sustava Sunda – Java, gdje međudjelovanje geometrije ploče, strukture kore i deformacije gornje ploče upravljaju regionalnom tektonikom i seizmičnošću. Naše istraživanje predstavlja integrirani geofizički prikaz orijentacija naprezanja, gravitacijskih anomalija, varijacija dubine moha i potpovršinskih struktura ispod Jave. Istraživanje se proteže na području otprilike 106° I – 114° I i 7° J – 10° J. Korišten je katalog potresa od 2000. do 2023. godine (48 825 događaja, raspon magnituda od 2,7 do 7,8 m_b, raspon dubine od 10 do 600 km) preuzet iz baze USGS-a, rješenja žarišnih mehanizama, orijentacije naprezanja određene na temelju pojedinačnih potresnih događaja, satelitski gravitacijski podatci, analiza radijalno usrednjenoga spektra snage (RAPS) za procjenu dubine moha i dvodimenzionalni refleksijski seizmički profili. Raspodjela seizmičnosti prikazuje Wadati-Benioffovu zonu koja je nagnuta prema sjeveru i otkriva relativno smanjenje pojavnosti potresa na srednjim dubinama ispod središnje Jave. Gravimetrijska interpretacija otkriva sustavne lateralne promjene gustoće i debljine kore, s velikim anomalijama duž južnoga ruba, malim anomalijama ispod sedimentnih bazena i lokalnim velikim anomalijama povezanim s vulkanskim područjima. RAPS analiza pokazala je da se dubina moha kreće od približno 11 do 40 km, što je u skladu s prethodnim regionalnim istraživanjima. Refleksijski seizmički profili dokumentirali su diskontinuitete reflektora i deformacije povezane s rasjedima, što je u skladu s frontalnim, zalučnim i rasjednim sustavima s horizontalnim pomakom unutar rubnoga sustava Sunda-Java.

Ključne riječi:
subdukcija Sunda-Java, seizmičnost, žarišni mehanizam, gravimetrijska anomalija, moho dubina (RAPS)

Author's contribution

Rian Amukti (Master): conceptualization, investigation, and software, writing – original draft, and writing – review & editing. **Lina Handayani** (Doctor): supervision. validation, writing - review & editing. **Sonny Aribowo** (Doctor): formal analysis, investigation, writing - review & editing. **Rashad A Bantan** (Professor): conceptualization, supervision. **Hamdy Aboulela** (Professor): methodology, writing - review & editing.
All authors have read and agreed to the published version of the manuscript.